NONSTATIONARY PRODUCTIVITY IN GLOBAL FISH STOCKS

by

Gregory L. Britten

Submitted in partial fulfillment of the
requirements for the degree of
Master of Science

at

Dalhousie University
Halifax, Nova Scotia
September 2014

M.S.Y.

Resurrected: 2014

Here awakens M.S.Y.

Reborn again, but far more spry

It dips, it dives, its hot, its cold

Just keep watch or we'll quick lose hold

Table of Contents

List of Tables

List of Figures

Abstract

Environmental change in the ocean has raised significant concern over the continued productivity of global fisheries resources. In this thesis, I investigate time-varying rates of population growth and biomass production (i.e. 'nonstationary productivity') in global fish stocks by analyzing a new global database of fisheries time series. Using Bayesian population models, I describe nonstationary productivity in individual stocks, and then synthesize results at regional, taxonomic, and global scales. I demonstrate significant regional and global trends in two aspects of stock productivity: juvenile recruitment (the production of individual fish) and total productivity (the production of stock biomass). Importantly, these declines can be explained by changes in temperature, phytoplankton, and the intensity of historical overfishing. Further, observed trends are shown to significantly alter rebuilding timelines for depleted stocks. These results help track the historical trends and current status of stock productivity and reveal key environmental drivers at the regional and global scale.

List of Abbreviations and Symbols Used

AIC	Akaike Information Criteria
α	Maximum reproductive rate
B	Total biomass (in kilograms)
B:B_{MSY}	Ratio between observed and target biomass
β	Strength of density dependence
BIC	Bayesian Information Criteria
C	Catch (in kilograms)
c	Arbitrary numerical constant
CBD	Convention on Biological Diversity
CHL	Chlorophyll
CO_2	Carbon dioxide
$\frac{df}{dx}, \frac{d^2f}{dx^2}$	First and second derivative, respectively, of the function f with respect to variable x
Δx	Greek 'Delta' notation representing the change in variable x
e	Euler's constant
e	Vector of residuals
EBFM	Ecosystem Based Fisheries Management
F	Annual fishing mortality
K	Carrying capacity of a population
L	Statistical likelihood
$\hat{x}$	'Hat' notation, representing an empirical estimate of x
LME	Large Marine Ecosystem
MAD	Median Absolute Deviation

MAP	Maximum a posteriori
MCMC	Markov Chain Monte Carlo
MLE	Maximum Likelihood Estimate
MSY	Maximum Sustainable Yield
n	Number of stocks
P	P.value
R	Recruitment
r	Intrinsic total productivity
R^2	Coefficient of determination
R_{MAX}	Maximum recruitment potential
σ, σ^2	Standard deviation and variance, respectively
SST	Sea Surface Temperature
T	Length of time series
τ	Lag (years) between spawning and recruitment
θ	Estimable parameter
VPA	Virtual Population Analysis

Acknowledgements

The scientific results in this thesis owe most thanks to four people. To my supervisors, Boris Worm and Mike Dowd for providing me with the perspective, skills, and inspiration to tackle a big topic. To Cóilín Minto for getting me started in fisheries science and teaching by example, and for beginning the work on nonstationary productivity. And to Ransom A. Myers (RAM), whom I never met, but from whom I have learned greatly though his students and papers. His research launched a new era in population biology with the development and statistical analysis of large global databases, which ultimately forms the basis of this work.

My own scientific journey at Dalhousie has been shaped most by former members of the Worm/Lotze/Jonsen FMAP lab; namely, Boris Worm, Heike Lotze, Ian Jonsen, Coilin Minto, Daniel Ricard, Francesco Ferretti, Wade Blanchard, Sean Anderson, Christine Ward-Paige, Camilo Mora, Catherine Muir, Arliss Winship, Derek Tittensor, Greg Breed, Trevor Davies, Anna Magera, Stephanie Boudreau, and Marta Coll. FMAP was an exciting time for me and marks the start of my scientific career. Heike, in all her patience, was kind enough to let me play shadow to a superstar team while early in my very green undergraduate years. I can't overstate how motivating that period in my life was.

Finally to Sarah, who supports me in so many ways and lightens my life with her sense of humour. As much as I hate to admit it, she is always killin' the jokes.

Chapter 1

Introduction

A hallmark of human prosperity is the sustainable exploitation of natural ecosystems and their biological resources. Wild marine fisheries are a central example which provide a significant source of animal protein for more than half of the world's population [1]. Numerically, wild fisheries produce roughly 90 million tonnes of consumable biomass per year [1]. That equals an *annual* quantity of food greater than $\frac{1}{3}$ of the entire human biomass on earth [2]. However, observations and predictions of global climate change increasingly suggest fundamental shifts in ecosystem productivity which may impact our ability to sustainably exploit fisheries resources. For example, atmospheric CO_2 accumulation over the 21st Century is predicted to cause accelerated ocean warming [3], acidification [4, 5], deoxygenation [6, 7], and sea-level rise [8]; all of which impose dramatic, yet poorly understood consequences for the health of fish populations [9–11] and their supporting marine ecosystems [5, 12]. Basic ecological research has focused on responses to climate forcing with increasing recognition of *nonlinear* and *nonstationary* response processes, including state-shifts [13], critical transitions [14], and environmental regime-shifts [15]. Analytical work has also become a priority with efforts to understand nonstationary processes using empirical analyses such as early warning signs [14, 16, 17], critical slowing-down [18], and 'flickering' [18, 19]. Taken together, modern evidence suggests that nonstationary ecological processes are the rule, rather than the exception in contemporary ecosystems, with important but poorly constrained consequences for fisheries productivity.

In practical terms, nonstationary processes suggest that past ecological data may be unrepresentative of current ecosystems, which has dangerous consequences when trying

to make predictions and sustainably exploit populations. This situation was summarized more than 25 years ago and echoes even more loudly today:

> Hidden in most of the literature on fisheries modelling and stock assessment is the assumption that there are stationary relationships between key rate processes and population size measures. By stationarity, I mean a relationship that may be clouded by white, serially uncorrelated, noise, but has a statistically invariant distribution of rate variables for each value of the state variable. So we blithely fit long time series of stock-recruitment data as though the older recruitment observations were still representative of what similar spawning stock sizes would produce today, we plug growth curves estimated 10 years ago into yield-per-recruit analyses, and pretend in the analysis of catch at age data that natural mortality rates have been constant through time.
>
> - Carl Walters (1987; *CJFAS*; [20])

Despite the recognition of nonstationary processes, it is less clear how to empirically model and predict such processes in the context of fisheries. In theory, the strategy should be both *adaptive* and *ecosystem-based*, designed to fluidly incorporate new quantitative biological knowledge when ecological conditions change. But in practise this remains a major challenge. Here I propose a particular strategy based on adaptive single species models and Bayesian probability. Conceptually, the core methodology makes use of time-varying extensions of classical production models in which key production rate parameters are treated as dynamic latent state variables. The latent productivity state is described by a probability distribution and dynamically updated on account of new observations. As I will explore in the thesis, there are well-developed statistical tools to infer and predict such states based on *sequential Bayesian updating* [21–24]. My goal is to empirically apply these methods to a new global database of fisheries time series [25] and to describe nonstationary fish stock productivity at the broadest possible scale. I first assess the magnitudes, spatiotemporal patterns, and potential drivers of nonstationary productivity, and then characterize the consequences for key management outcomes such as rebuilding time

lines for depleted stocks.

Structure of the thesis

In this thesis, I apply sequential Bayesian updating to extend two canonical fisheries models to the nonstationary case. The goal is to apply these models to all available fisheries time series [25] and then synthesize nonstationary productivity using meta-analyses at the regional, taxonomic, and global scales. The nonstationary models describe two distinct aspects of productivity, juvenile recruitment and total biomass production. Each process is quantified by a small number of fundamental biological parameters which govern stock production rates and feed directly into traditional management. The Bayesian extensions allow these parameters to vary in time and are sequentially updated on account of new time series data. In this sense, key biological parameters are observationally tracked as dynamic states analogous to weather tracking and prediction. The research is primarily a synthesis of three fundamental components: simple population models and well-understood statistical methods, applied to a publicly available global database of fisheries time series - the RAM Legacy Stock Assessment Database (www.ramlegacy.org).

In Chapter 2, I focus on nonstationary recruitment capacity by extending the well-known Ricker model which governs the production dynamics of juvenile offspring as a function of adult biomass. The magnitude of annual recruitment is highly variable, yet it provides the basis for population growth and stock productivity by determining the initial number of fish that may grow, die, or be harvested by the fishery [26]. Recruitment capacity is described by two parameters: α, the maximum reproductive rate, and β, the strength of population density-dependence. After selecting 262 appropriate stocks from the RAM database, I tested for significant variability in these parameters and then quantified the magnitudes of trends. I summarized patterns by global, regional, and taxonomic grouping by performing a post-hoc meta-analysis of linear slopes. I then related

these patterns to regional trends in environmental and fishing-related variables.

In Chapter 3, I investigate global patterns of nonstationary total productivity by extending the Graham-Schaefer model to infer variation in the intrinsic productivity parameter r which combines recruitment, individual growth, and natural mortality. Using time series from 211 assessed stocks I quantified variability in r using sequential Bayesian updating and summarized regional, taxonomic, and global patterns. I then calculated the consequences for the rebuilding potential for 147 of the 211 stocks currently below their target biomass levels and estimated probabilistic rebuilding timelines on the basis of contemporary productivity.

In Chapter 4, I conclude the thesis with a discussion of the broader implications of the results, focusing on areas of follow-up research.

Chapter 2

Environmental change drives declining recruitment capacity in global fish stocks*

Abstract

It has recently been shown that marine fish and invertebrates are shifting their regional and global distributions in response to climate change, but it is unclear whether their productivity is being affected as well. Future projections of climate impacts on productivity are varied, while past changes due to documented environmental trends and the biological legacy of historical overfishing remain unresolved. Here we applied dynamic linear models with time-varying biological parameters to analyze time series from 262 fish stocks of 127 species in 39 large marine ecosystems and high-seas areas (hereafter LMEs). We discovered widespread changes in the relationship between population size and the production of juvenile offspring (recruitment), suggesting fundamental biological change in fish stock productivity across broad spatial and temporal scales. Globally, we estimate that recruitment capacity has declined by approximately 3% per decade relative to the historical maximum. However there is an observed contrast between highly negative trends in the North Atlantic and more neutral patterns in the North Pacific. Most importantly, the extent of biological change in each LME was significantly related to regional ocean warming, declining phytoplankton biomass, and the intensity of historical overfishing in that ecosystem. We conclude that observed environmental change over the last 50-100 years has already compromised the productive capacity of stocks at the recruitment stage

*In review at time of submission as: Britten GL, M Dowd, B Worm. 2014. Environmental change drives declining recruitment capacity in global fish stocks. *Nature*

of the life cycle. These results provide an empirical baseline for ecosystem-based fisheries management and may help revise expectations for future food production from the oceans.

2.1 Introduction

Human well-being is closely linked with the productivity of marine fisheries, which provide a significant source of protein for more than half of the world's population [1]. However, climate change may increase or decrease productivity through a variety of physical and biological mechanisms, including larger habitat areas for temperate species [27], altered body sizes [28], food availability [29], and increased exposure to oxygen-depleted and acidic waters [5]. Recent research has documented marked changes in the distributional patterns of marine species that are consistent with climate forcing [30, 31]. However, it is not empirically understood whether environmental changes [29,32,33] are already affecting the productive capacity of populations at a global scale, or whether stocks are biologically compromised due to the long-term selection effects of historical overfishing [34, 35]. Here we address this question by evaluating trends in the relation between the size of the adult population (or spawning stock) and annual production of juvenile offspring (recruits) using a new global database of stock-recruit time series [25]. We then relate recruitment patterns to environmental variables associated with temperature, phytoplankton abundance, and historical overfishing.

Fisheries scientists model recruitment with simple mathematical functions that relate the quantity of spawning stock biomass to the annual production of recruits. The magnitude of annual recruitment is highly variable, yet it provides the basis for population growth and stock productivity by determining the initial number of fish that may grow, die, or be harvested by the fishery [26] (i.e. total productivity is the product of recruitment, individual growth, and mortality). As such, the stock-recruit relationship has been identified as 'the most important and generally most difficult problem in the biological

assessment of fisheries' [26]. The most commonly used recruitment function is the well-known Ricker model

$$R_t = \alpha B_{t-\tau} e^{-\beta B_{t-\tau}},$$

where recruitment R at time t is an increasing function of the spawning stock biomass B (lagged by the age of recruitment τ), with negative exponential density-dependent feedback. The two model parameters, α and β, characterize the magnitude of recruitment, where α is the maximum reproductive rate (or density-independent recruitment) and β gives the rate at which recruitment is reduced by density-dependent feedbacks. These two parameters combine to give the maximum recruitment capacity for an individual stock when $\frac{dR}{dB} = 0$ and $\frac{d^2R}{dB^2} < 0$, yielding

$$R_{MAX} = \frac{\alpha}{\beta} e^{-1},$$

where e is Euler's constant. Note that R_{MAX} is a measure of inherent biological productivity, and is independent of actual biomass.

When recruitment models are fitted to data (Figure 2.1A-F) there is often considerable structure in the residual variation (Figure 2.1G-I) which suggests that time-varying ecological processes have affected the stock-recruit relationship. Trends can be observed as directed declines (Figure 2.1G), threshold-like dynamics (Figure 2.1H), or regime shifts (Figure 2.1I; note that the observed shift coincided with the 1977 reversal of the Pacific Decadal Oscillation [15]). We quantified the time variability in the stock-recruit relationship using a dynamic linear model (DLM) representation of the Ricker model, allowing the biological parameters to vary in time [36, 37], i.e. $\{\alpha, \beta\} \rightarrow \{\alpha_t, \beta_t\}$. We combined these parameters to evaluate changes in R_{MAX} for individual stocks, where ΔR_{MAX} represents

the linear slope for an individual stock over time, standardized relative to the historical maximum. Using meta-analytic methods, we averaged individual ΔR_{MAX} across multiple stocks at the ecosystem and taxonomic level (denoted ΔR^k_{MAX} to indicate the average across grouping k) and then related these to regional trends in sea surface temperature (ΔSST [32]), chlorophyll (ΔCHL [29], a widely-used a proxy of phytoplankton biomass), and a measure of historical overfishing (taken as the average ratio of historical stock biomass to target biomass [25], denoted $B{:}B_{MSY}$). See Appendix A for detailed methodology.

2.2 Results

We found the stock-recruitment data supported time-varying recruitment capacity (R_{MAX}) for 79% ($n = 208$) of stocks according to model selection (Figure 2.2). Of these, 69% ($n = 139$) showed negative trends (Figure 2.2). For all stocks combined, ΔR^k_{MAX} was estimated at approximately -3% per decade ($P < 0.001$, Figure 2.2D). However there was a broad-scale divergence in values between the North Pacific and North Atlantic oceans, with the North Atlantic showing steeper declines. In contrast, the North Pacific showed approximately neutral trends across 4 LMEs, each with a relatively large number of stocks. Across all LMEs, we estimated that 31 out of all 39 LMEs (79%), and 20 out of 27 LMEs with >3 assessed stocks (74%), showed negative ΔR^k_{MAX} (Figure 2.2). The most positive value was found in the Gulf of Mexico, while the heavily depleted Newfoundland and Labrador LME showed the most negative value (Figure 2.2B). At the taxonomic level, groundfish (bottom-associated species such as flatfishes, *Pleuronectiformes*, and cod-like *Gadiformes*) showed the most negative ΔR^k_{MAX} (Figure 2.2C). At the species level, the most negative values were observed for several North Atlantic species such as American plaice (*Hippoglossoides platessoides*), European plaice (*Pleuronectes platessa*), common European sole (*Solea vulgaris*), and Atlantic cod (*Gadus morhua*). In the North Pacific,

however, many groundfish species showed opposite patterns, with stocks of rex sole (*Glyptocephalus zachirus*), flathead sole (*Hippoglossoides elassodon*), and arrowtooth flounder (*Atheresthes stomias*) trending positively. Pelagic (open-water) species such as herring (*Clupea harengus*, *C. pallasii*) and swordfish (*Xiphias gladius*) often showed ΔR^k_{MAX} values closer to zero.

In general, we found individual stock-recruit parameters changed in a way that resulted in stronger density-dependent processes and reduced maximum reproductive rates. Of individual stocks with negative ΔR_{MAX}, 71% displayed more negative β parameters and 29% experienced declining α. We also found that ΔR_{MAX} was generally independent to the assumed form of density-dependence in the stock-recruit model, or to whether the model let α or β vary in time, indicating robustness in these estimates (see Appendix A for details and sensitivity analyses).

Importantly, trends in recruitment capacity were found to be significantly related to environmental and fishing-related variables (ΔSST, ΔCHL, B:B_{MSY}) across all LMEs (Figure 2.3). Considering all species together (Figure 2.3A), ΔR^k_{MAX} in each LME was positively associated with ΔCHL and negatively associated with ΔSST in that ecosystem (Figure 2.4A,B), and accounted for 27% of the total variance (as measured by adjusted R^2). Again, an interesting contrast emerged between trends in the heavily exploited groundfish (combining orders *Pleuronectiformes* and *Gadiformes*, Figure 2.3B) and the predominantly pelagic *Perciformes* and *Clupeiformes* (Figure 2.3C). For groundfish, ΔR^k_{MAX} was significantly related to changes in temperature (ΔSST, Figures 2.3B & 2.4A), phytoplankton biomass (ΔCHL, Figure 2.4B), and the historical intensity of exploitation (mean B:B_{MSY}, Figure 2.4C). These three variables explained 76% of the variance across these species, representing 21 LMEs. Variation in the more pelagic taxa (combining *Perciformes* and *Clupeiformes*) was mostly related to ΔSST (Figures 2.3C & 2.4A), which explained 41% of the variance across 23 LMEs. To evaluate more recent changes, we also assessed these relationships using data since 2000 only (see Appendix A).

These results were consistent with the overall findings and gave similar trends in recruitment capacity with highly significant relationships to environmental drivers, including a negative effect of ΔSST and positive effect of ΔCHL for all stocks combined.

2.3 Discussion

Taken together, these results provide empirical context for understanding contemporary changes in the productivity of fish stocks. To date, forecasts of fisheries productivity under future climate change scenarios have varied in their predictions. For example, the productivity of temperate species has been projected to increase 30-40% based on expansion of fish habitat and increased primary productivity [27], while models of individual fish metabolism predict shrinking body sizes with warming oceans [28] which could affect fecundity and productivity. Here we utilized the history of recorded stock-recruitment data to show that observed environmental changes already have negative impacts on the recruitment stage of the life cycle. However, we caution that these trends in recruitment biology should be combined with other model-based forecasts that weigh factors related to habitat quantity and quality to more fully determine expected change in both biomass distribution and productivity. We further note that the drivers of recruitment capacity identified here likely vary in importance among stocks and regions. Changes in temperature, plankton concentration, and overfishing are all known to affect recruitment in sometimes complex ways, including effects at both the adult (e.g. maternal effects on recruitment [38]) and larval stages (e.g. environmental effects on hatching and survival [39]). Our results make neither assumptions nor inferences regarding specific mechanisms. It is imperative that additional, local-scale analysis be performed to understand how specific drivers interact to drive the recruitment capacity of individual stocks.

At larger scales, the apparent divergence in productivity among the North Pacific and North Atlantic provides an interesting contrast. The North Pacific experienced a

broad-scale oceanographic regime shift in the 1970s [15], which resulted in relatively flat long-term environmental trends (Figure 2.4). Observed patterns suggest that recruitment capacity may have tracked this variability (e.g. Figure 2.1I), resulting in small ΔR_{MAX} values overall. Shorter histories of exploitation and lower exploitation rates [40] are also likely to have tempered declines in this region due to overfishing. In contrast, the North Atlantic is marked by strong directional environmental change and long-term overexploitation (Figure 2.4). Environmental and fishing-related trends in this region were among the most severe across all three variables (ΔSST, ΔCHL, B:B_{MSY}) and were closely related to ΔR_{MAX}. An exception for the North Atlantic is the positive ΔR_{MAX} in the Gulf of Mexico (which mostly predates the Deepwater Horizon spill in 2010 [41]). It is important to note that the relative scarcity of stock assessments in other regions of the world (grey areas in Figure 2.4C and see [25, 42]) limits our understanding of global fish populations as a whole.

In addition to impacting the productivity of marine fish stocks, observed changes in recruitment parameters may also have consequences for the stability of populations. Recent theoretical work has linked observed patterns of population stability [43] to changes in stock-recruitment parameters [44] due to age-selective fishing. It was hypothesized that population stability has decreased in stocks due to increases in the mean and variance of the maximum reproductive rate α caused by the truncation of population age structure by fishing. Our results, however, suggest that such increases in α are not often observed in assessed fish populations, where α has generally trended downward. Rather, frequently observed increases in the magnitude of the density-dependent parameter β may provide an alternative explanation for reduced stabilities in exploited stocks based on the well-known destabilizing effects of strong density-dependent feedbacks [45].

In summary, empirically estimated trends in recruitment capacity (Figures 2.1 & 2.2) provide strong evidence for climate- and fishing-related changes in the productivity of

marine fish stocks (Figure 2.3). These shifts are significantly related to ongoing environmental and biological change at the ecosystem scale; specifically changes in sea surface temperature, phytoplankton biomass, and the history of stock biomass depletion (Figure 2.4). The reality of time-varying biological parameters requires managers to revisit the common assumptions of fixed maximum sustainable yields [20] and emphasizes the need for ecosystem-based management strategies that investigate and account for observed environmental and fishing-related impacts on the population dynamics of fish stocks. Such strategies are a prerequisite to ensuring the successful rebuilding and sustainable harvesting of fisheries resources in a rapidly changing environment.

2.4 Figures

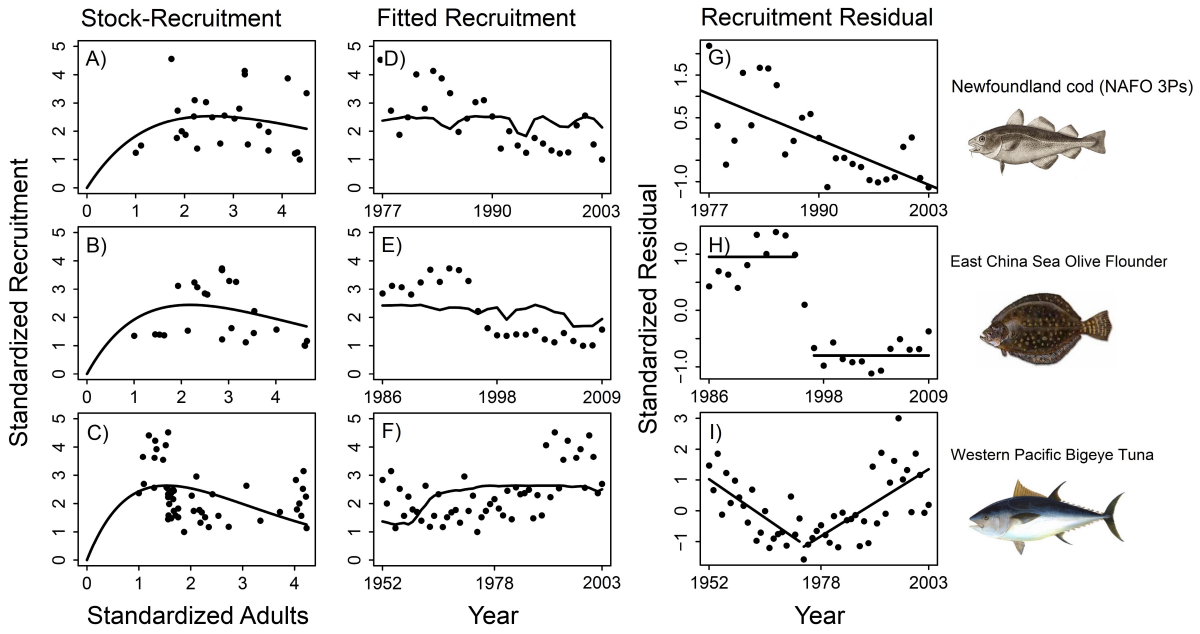

Figure 2.1. Patterns in stock-recruitment data. Ricker models fitted to stock-recruitment data (A-C) often display systematic errors (D-F). Model residuals can show diverse behaviours, including progressive declines (G), abrupt thresholds (H) or reversing regime shifts (I). Data are standardized to have unit variance.

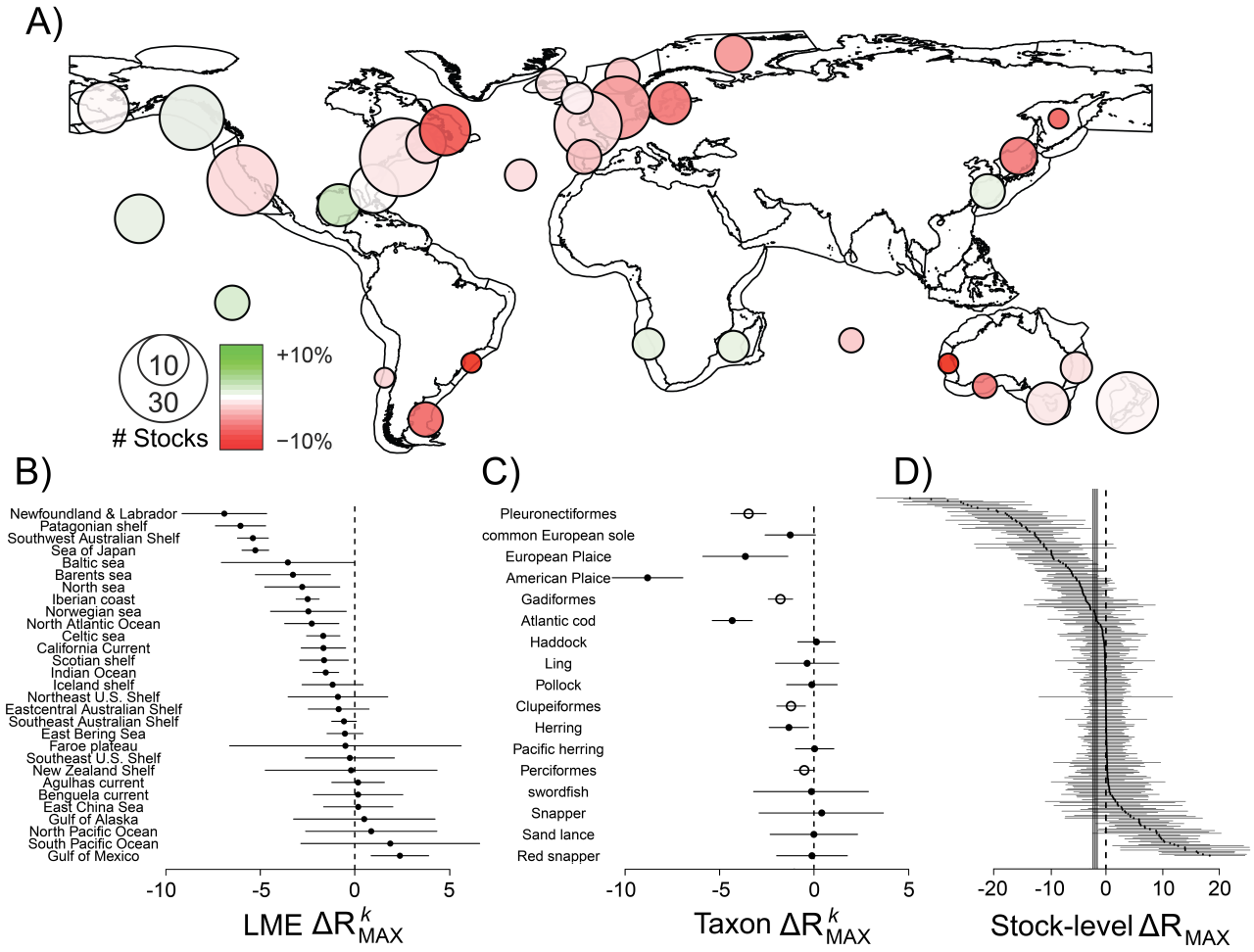

Figure 2.2. Meta-analysis. Standardized trends in recruitment capacity (ΔR_{MAX}; units % change R_{MAX} per decade, relative to the historical maximum). (A) ΔR^k_{MAX} (representing the meta-analytic average ΔR_{MAX}) by large marine ecosystem (LME) containing > 3 assessed stocks. The color of the circle gives the direction and magnitude of ΔR^k_{MAX} and the size of the circle gives the number of stocks in the LME. (B) Meta-analytic ΔR^k_{MAX} per LME and standard error. (C) Taxon-level ΔR^k_{MAX} for species with > 3 assessed stocks (dark circles) and by taxonomic order (open circles). (D) All 262 individual stock ΔR_{MAX} with the grand meta-analytic mean ($P < 0.001$) and standard error (shaded bar). Meta-analytic means were derived by averaging the individual stock trends by inverse-variance weighting.

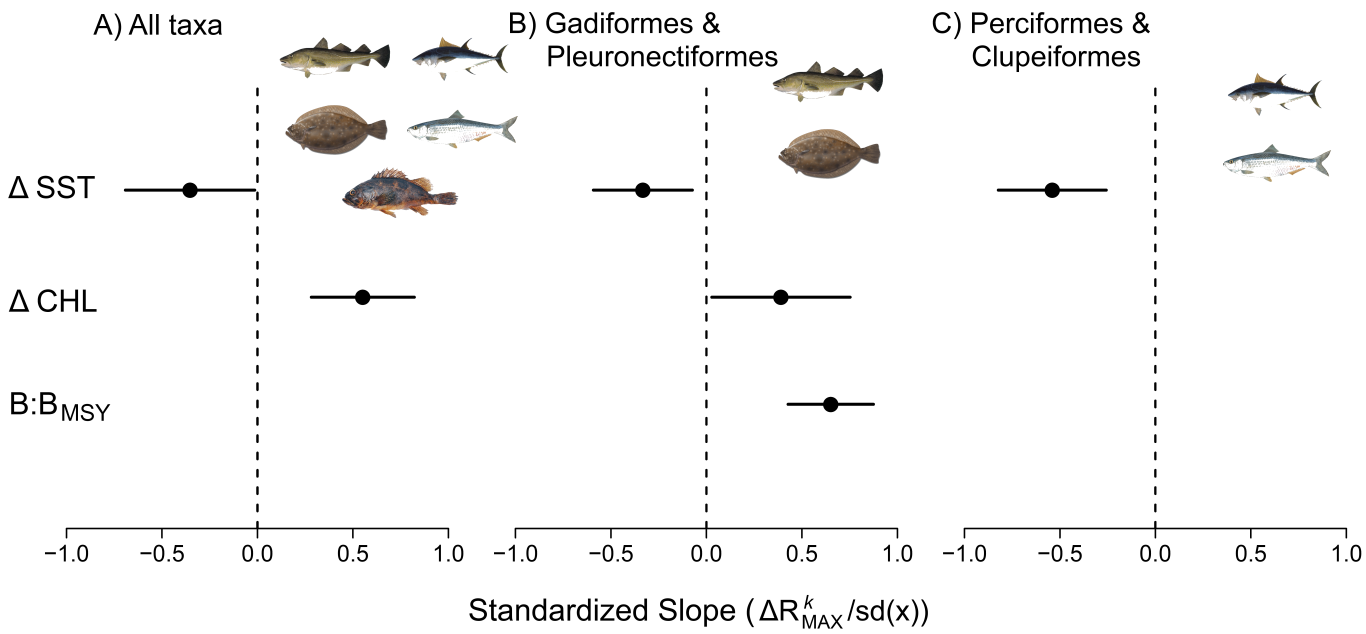

Figure 2.3. Drivers of recruitment capacity. Relationships between LME-level ΔR^k_{MAX} and environmental and fisheries variables using weighted multiple regression (weighted according to the number of stocks in the LME). The regression variables were selected using BIC. The three LME-specific covariates included: i) trends in sea surface temperature (ΔSST), ii) trends in chlorophyll concentration (ΔCHL), and iii) the historical mean ratio of stock biomass to target biomass ($B:B_{MSY}$). The regression slopes were normalized by transforming the regression variables to unit variance.

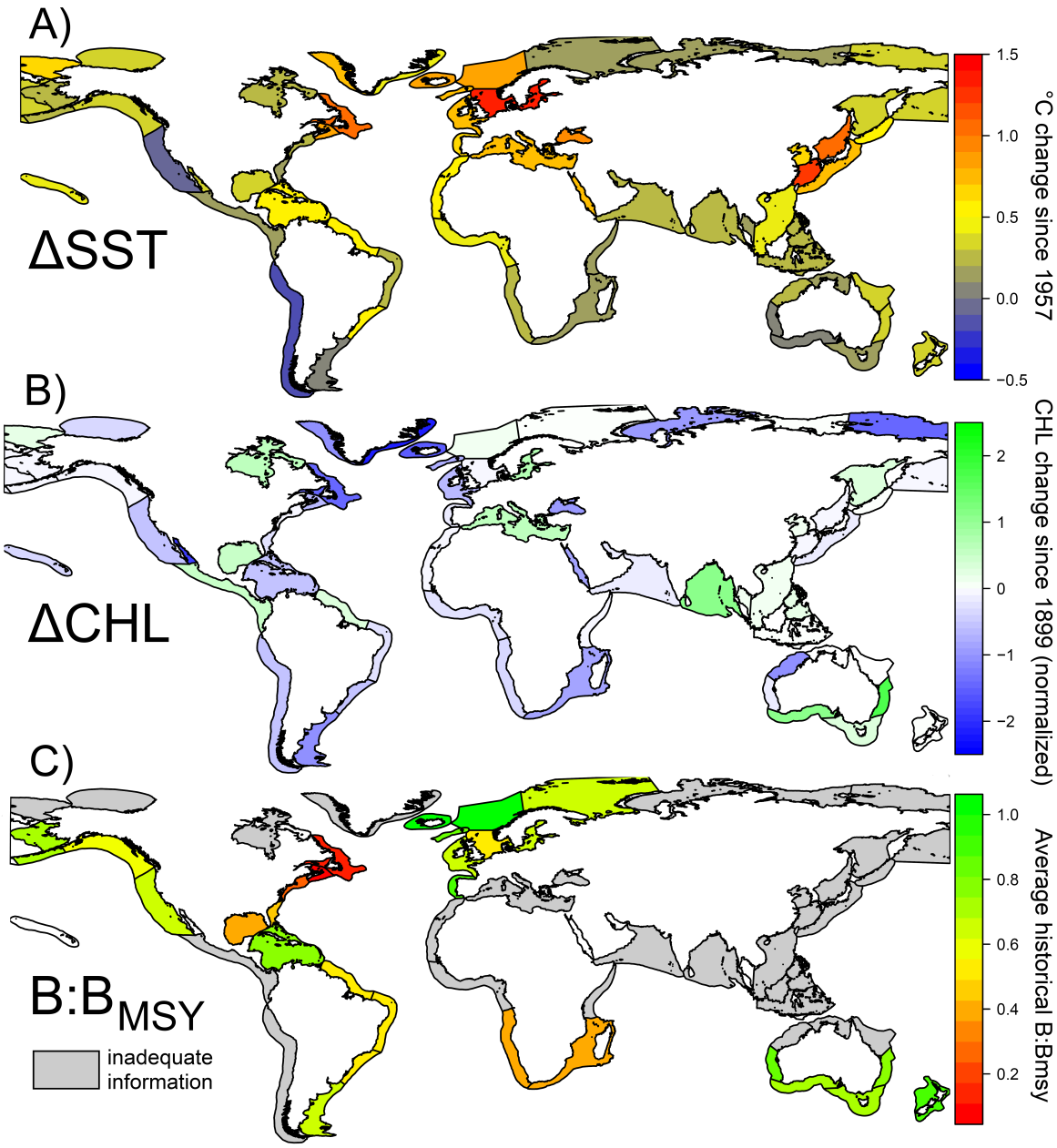

Figure 2.4. Spatial distribution of environmental drivers by LME. Linear trends in sea surface temperature (ΔSST; Panel A; [32]) span the period 1957 – 2009. Linear trends in chlorophyll concentration (ΔCHL, used as a common proxy for phytoplankton biomass; Panel B; [29]) span the period 1899 – 2010, and, where available, the historical ratio of biomass to target biomass(B:B_{MSY}; scaled between 0-1); Panel C; [25]) span the period of formal stock assessments on a stock-by-stock basis.

Chapter 3

Rebuilding global fisheries under nonstationary productivity*

Abstract

After a long history of overexploitation, the rebuilding of global fish stocks has become a major international management goal and an explicit Convention on Biological Diversity (CBD) target for 2020. The objective is to rebuild depleted stocks to biomass levels that produce maximum sustainable yield (MSY), i.e. B_{MSY}. However, it has recently been shown that a fundamental component of productivity, juvenile recruitment, has experienced highly nonstationary behaviour in recent decades, with currently unknown consequences for total productivity (i.e. the annual production of biomass). We evaluated nonstationary productivity by developing a Bayesian production model with time-varying intrinsic productivity parameter r, which determines both the magnitude of MSY and timescales of population rebuilding. We inferred nonstationary productivity from observed biomass time series of 211 assessed stocks and evaluated current rebuilding times to B_{MSY} for 147 currently depleted stocks. Results reveal significant changes in productivity over time with 60% of stocks showing variation in r of 10% per year, or more, leading to long systematic periods of previously unrecognized over- or underfishing. We further show that the nonlinear dependence between rebuilding time and r causes a highly skewed rebuilding time distribution when nonstationary parameters are taken into account. These results indicate that the rebuilding of many depleted stocks will be longer than previously thought due to dynamic variation and uncertainty in key parameters.

*Prepared for submission as: Britten GL, M Dowd, L Kanary, B Worm. 2014. Rebuilding global fisheries under nonstationary productivity. *PNAS*

More stringent controls on fishing mortality and an adaptive management approach that accounts for nonstationary productivity are required to rebuild stocks and meet international biodiversity targets.

3.1 Introduction

With widespread recognition of the economic and ecological risks caused by progressive fisheries depletion [40,46,47], scientists and policy makers have shifted focus to the rebuilding of depleted stocks [40, 48, 49]. Rebuilding initiatives have received major international support, beginning with the Magnuson-Stevens act in the United States, which legally mandates a ten year rebuilding plan for all depleted stocks [49] followed by major fisheries reform in Europe [50], and the declaration of an explicit Convention on Biological Diversity (CBD) rebuilding target for 2020 [51]. Such explicit timelines require a fundamental understanding of both rebuilding potential and productivity dynamics in global fish stocks; however, the increasing realization of rapid environmental change affecting fish population dynamics [7, 29, 32] suggests that rebuilding potential may be a moving target.

From a management perspective, dynamic changes in productivity challenge the appropriateness of rebuilding times estimated on the basis of historical data [20]. For example, environmentally driven regime-shifts are now recognized as a pervasive ecological phenomenon [13, 14, 52] and have been shown to widely impact fish populations [53]. Furthermore, a recent global meta-analysis of recruitment capacity (which couples with growth and mortality to set total productivity) found that many regions of the world show significantly declining recruitment capacity over the last several decades, linked to warming ocean temperatures, declining phytoplankton abundance, and historical overfishing [54]. With the backdrop of climate change, these nonstationary ecological processes

present managers with tremendous uncertainty with respect to current and future productivity and rebuilding times estimated therefrom. Most previous analyses, however, assume stationary productivity [20, 48, 49] and may not reflect current conditions.

Here we investigated global patterns of nonstationary total productivity by reconstructing historical patterns of variation and uncertainty in the intrinsic productivity parameter r, arguably the most fundamental parameter in population ecology and fisheries management. We first quantified the extent of nonstationary productivity among 211 assessed stocks (147 of which are depleted below B_{MSY}) from the global RAM Legacy Stock Assessment database [25] and then estimated Bayesian rebuilding time distributions under various fishing levels on the basis of current productivity.

Specifically, we extended the well-known Graham-Schaefer surplus production model [48, 49, 55] to allow the intrinsic productivity parameter r to vary as a latent stochastic process

$$B_{t+1} = B_t + r_t B_t \left(1 - \frac{K}{B_t}\right) - C_t,$$

where B is the total biomass at times t and $t+1$, K is the carrying capacity, C is the catch and the time-varying intrinsic productivity r_t is parameterized as a random walk with constant slope, $r_{t+1} = r_t + \Delta r + e_t^r$ where Δr is the time-invariant slope and e_t^r is a Gaussian variable with variance σ_r^2 (see Methods). The latent intrinsic productivity was fitted to observed stock biomass and catch series using Bayesian state space methods based on Kalman filtering and smoothing [23, 24]. The basic concept is to treat r_t as a hierarchical state variable which varies along with B and C and use the time series to update the probability distribution sequentially over time. We first applied the analysis to each individual stock and then aggregated the stock-specific results at the level of

Large Marine Ecosystem (LME) and taxonomic order to investigate broader-scale patterns of variability. To characterize contemporary intrinsic productivity, we averaged over the posteriors of the last five years for each inferred r_t series. Based on contemporary productivity, we then calculated the probabilistic predictive posterior rebuilding time distribution for each stock by varying levels of annual fishing mortality, denoted F.

3.2 Results

The analysis revealed that intrinsic productivity was highly variable across stocks and often deviated widely from predictions based on static parameters (Figure 3.1). Trends were regularly observed as long term directional change (e.g. Figure 3.1A,B) or regime shifts (e.g. Figure 3.1C,D) which diverged from stationary models for decadal periods or longer. Such behaviours indicate that fixed harvest strategies lead to systematic periods of historical over- and underfishing which are biased towards historically averaged productivity.

Across all stocks, we found that 60% of stocks exhibited variation in r_t of 10% per year or more. When aggregating regionally, we found that productivity has declined most in the Patagonian Sea, Faroe Plateau, and Australian LMEs (Figure 3.2B), although each of these regions is represented by limited samples (< 5 stocks). Other regions with declines were the Baltic Sea, Scotian and Iceland shelves (each with > 5 stocks available for analysis). Regions with increasing productivity included the Benguela and Agulas currents (3 stocks each) and the Gulf of Mexico (7 stocks). Taxonomically, there was less variation with trends centering near zero for most orders (Figure 3.2D). *Omeriformes* showed a large positive trend in r_t but this was highly variable across 4 stocks. *Perciformes* showed relatively consistent declines across 19 stocks but with magnitudes only slightly below zero. Across all stocks, there was no strong directional trend despite high interannual variability (Figure 3.2E,F). The overall maximum a posteriori (MAP) mean value of the

intrinsic productivity was estimated at $r = 0.39$ (Figure 3.2E) with the MAP mean annual rate of change estimated at approximately zero across all stocks (Figure 3.2F).

We also found that the most depleted stocks (i.e. the lowest $B:B_{MSY}$) are the ones with the lowest contemporary r_t values (Figure 3.3A). However, we found no relationship between stock status and rate of change in productivity (Figure 3.3B). This means that unproductive stocks tend to be the most currently depleted, but are not necessarily declining in productivity. The rebuilding contours show that rebuilding times are highly variable and strongly depend on the magnitude of fishing mortality (Figure 3.4). Under no fishing, 106 out of 133 stocks are predicted to recover within 10 years (i.e. the mode r_t predicts $t \leq 10$) rebuilding; Figure 3.4A). However that number drops to 60 out of 133 when fishing at 80% F_{MSY} (Figure 3.4B). A total of 14 stocks were estimated to have negative contemporary r_t and were not predicted to recover based on this calculation (grey area in Figure 3.4). When calculating rebuilding times based on probabilistic intrinsic productivity (Figure 3.5A), we found a highly skewed rebuilding distribution (Figure 3.5B). We applied this analysis to the 133 depleted stocks with positive contemporary productivity and found that the 95% credible interval often stretched to 20 or 30 years based on the characteristically strong positive skew (Figure 3.5C). This is a result of the nonlinear dependence between rebuilding time and contemporary productivity.

3.3 Discussion

In summary, the timeline for rebuilding depleted fish stocks will be determined by contemporary productivity which may not be reflected well by historical data (e.g. Figure 3.1). We have shown that intrinsic productivity r_t is highly variable in the majority of individual stocks, with diverse behaviours including slow linear changes and regime-shifts over time (Figure 3.1). The regular and persistent divergence between stationary and

nonstationary predictions indicates that management strategies based on fixed productivity are biased toward historical conditions and can lead to systematic historical over- and underfishing (Figure 3.1B,D). As a result, rebuilding times are set by the balance between current fishing mortality and contemporary productivity (Figure 3.4), leading to broad and highly skewed rebuilding time probabilities when nonstationary parameters are taken into account (Figure 3.5). These results suggest that rebuilding will be significantly delayed for many stocks and highlight the need for more decisive rebuilding plans that account for nonstationary ecosystem properties and fisheries productivity.

The increasing recognition of climate change and other nonstationary processes in ecology and fisheries forces the need for approaches to resource management that are adaptive [20] and ecosystem-based [56, 57]. A fundamental aspect of ecosystem-based fisheries management is the active maintenance of the supporting ecosystems to promote stock productivity [56]; however, adaptive management must also include quantitative strategies to update biological knowledge in the context of new ecosystem conditions [57, 58]. The general class of methods applied here (i.e. hierarchical state space models with dynamic biological parameters) provide intuitive and fully probabilistic methods for this based on sequential Bayesian updating. A major advantage of these methods is that they readily extend classical population and fisheries models to the nonstationary case. This way, key management parameters can be adaptively updated over time and integrated with pre-existing stock assessment theory and infrastructure. For example, target fishing mortality (F_{MSY}) may be dynamically updated as biological parameters change in response to ecosystem conditions.

The high variation in productivity is consistent with previous work on regime-shifts [53] and non-stationary recruitment capacity in global stocks [54]. However, weaker aggregated trends were observed in both our results (Figure 3.2) regime-shift analyses [53]. As a supplemental analysis, we correlated recruitment capacity slopes [54] with productivity slopes estimated here but found only a weak and insignificant relationship ($R^2 = 19\%$,

$P = 0.21$). It is possible that other ecological processes have compensated for declining recruitment (i.e. changes in somatic growth and mortality); however it is also possible that hidden stationarity assumptions [20] in the stock assessments lead to biomass estimates that are biased toward constant long term total productivity. Directly analyzing raw survey data with nonstationary methods may be needed to better identify relationships between total productivity, recruitment, mortality, and growth.

Given the rebuilding focus of global fisheries management, our work has demonstrated that nonstationary productivity may delay efforts to rebuild depleted stocks. Current meta-analyses of rebuilding still focus on static biological parameters [48, 49] which effectively capture mean productivity over the period of historical data. These timelines likely over- or underestimate rebuilding potential and the appropriate fishing levels for individual stocks and do not account for uncertainties with respect to biological change. In contrast, nonstationary models suggest much larger uncertainty bounds, indicating that many stocks will experience delayed rebuilding. We caveat this by acknowledging the simplicity of our biological model (Graham-Schaefer) which was chosen for generality rather than specificity; but note that it is still in regular use and forms the basis of more complex models [55]. At the individual stock level, our estimated rebuilding times are thus an approximation and should be followed up with more detailed stock-specific models.

In conclusion, nonstationary stock productivity has strong implications for the rebuilding timeline of global fisheries. Ignoring nonstationary processes risks over- and underfishing the resource and biases rebuilding times toward historical conditions which are increasingly unrepresentative of contemporary ecosystems. As nonstationary ecological behaviour is recognized as the rule rather than the exception, fisheries management needs to embrace adaptive methods and directly respond to varying environmental conditions. Our results suggest that such approaches will be required if we hope to rebuild stocks and meet international biodiversity targets in the face of rapid environmental change.

3.4 Figures

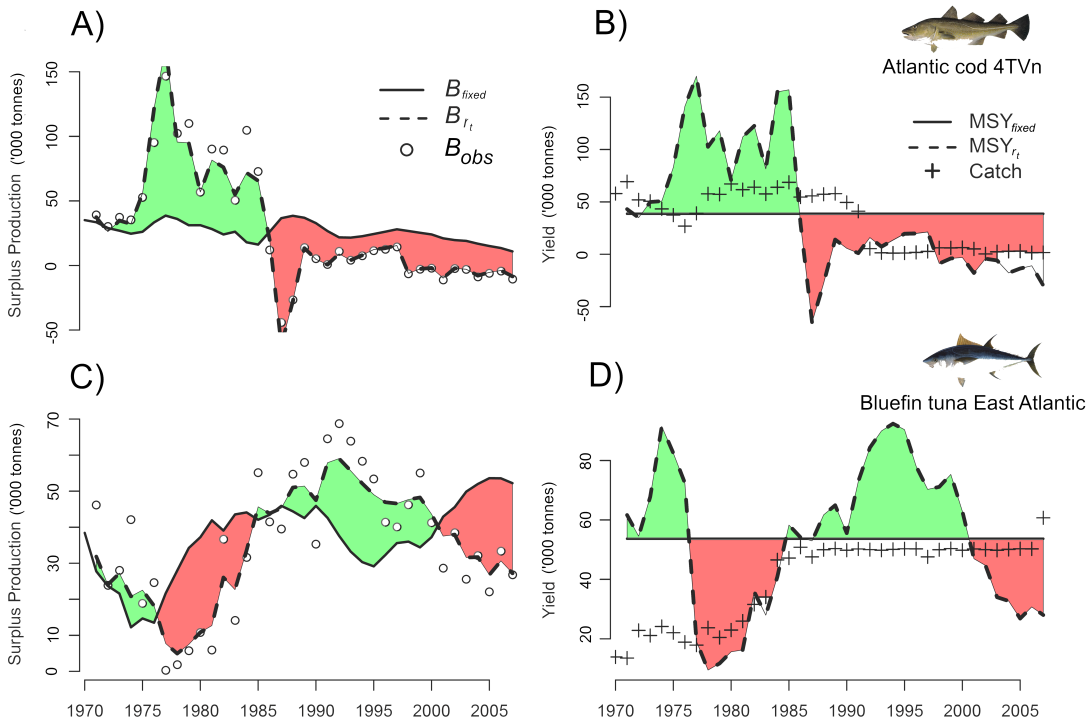

Figure 3.1. Examples of nonstationary stock productivity. Two example stocks (A-B: Eastern Scotian Shelf Atlantic cod, and C-D: Bluefin tuna from the East Atlantic) are shown fit with a stationary and nonstationary Graham-Schaefer model (fixed vs. time-varying intrinsic r, respectively). Panels (A, C) give the annual surplus production (open circles are observed values) while panels (B, D) give the theoretical maximum sustainable yield (crosses are recorded catches). The stationary model is shown with the solid line and the nonstationary model line is dashed. The green areas are where productivity is higher than would be predicted based on a stationary productivity and red is where productivity is lower. Note progressive decline in cod productivity and regime-like behavior in tuna.

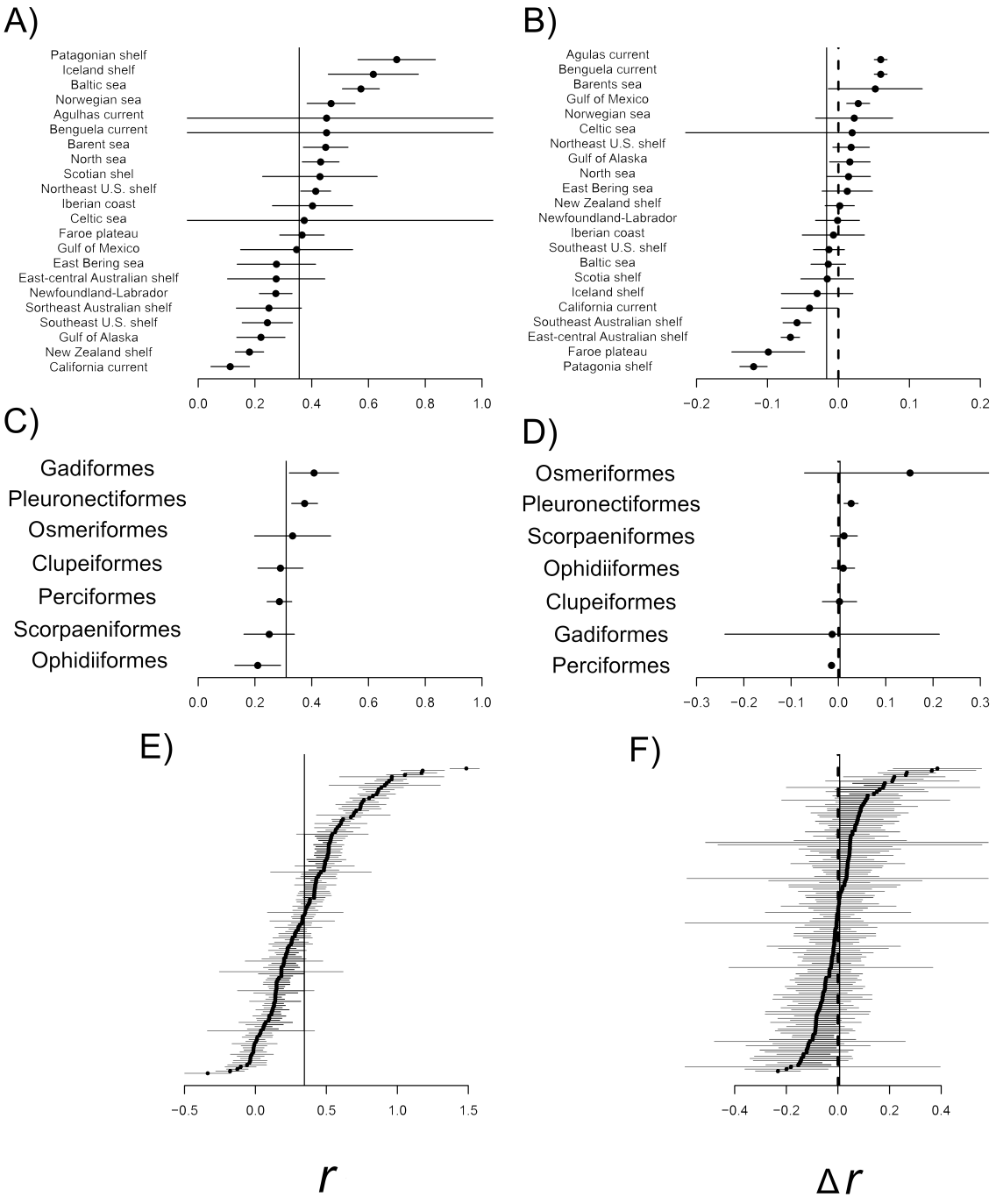

Figure 3.2. Meta-analysis of productivity. Panels show intrinsic productivity r and estimated rate of change Δr for Large Marine Ecosystems (A, B), major taxonomic orders (C, D), and all individual stocks (E, F). Solid line gives the grand median value for each grouping.

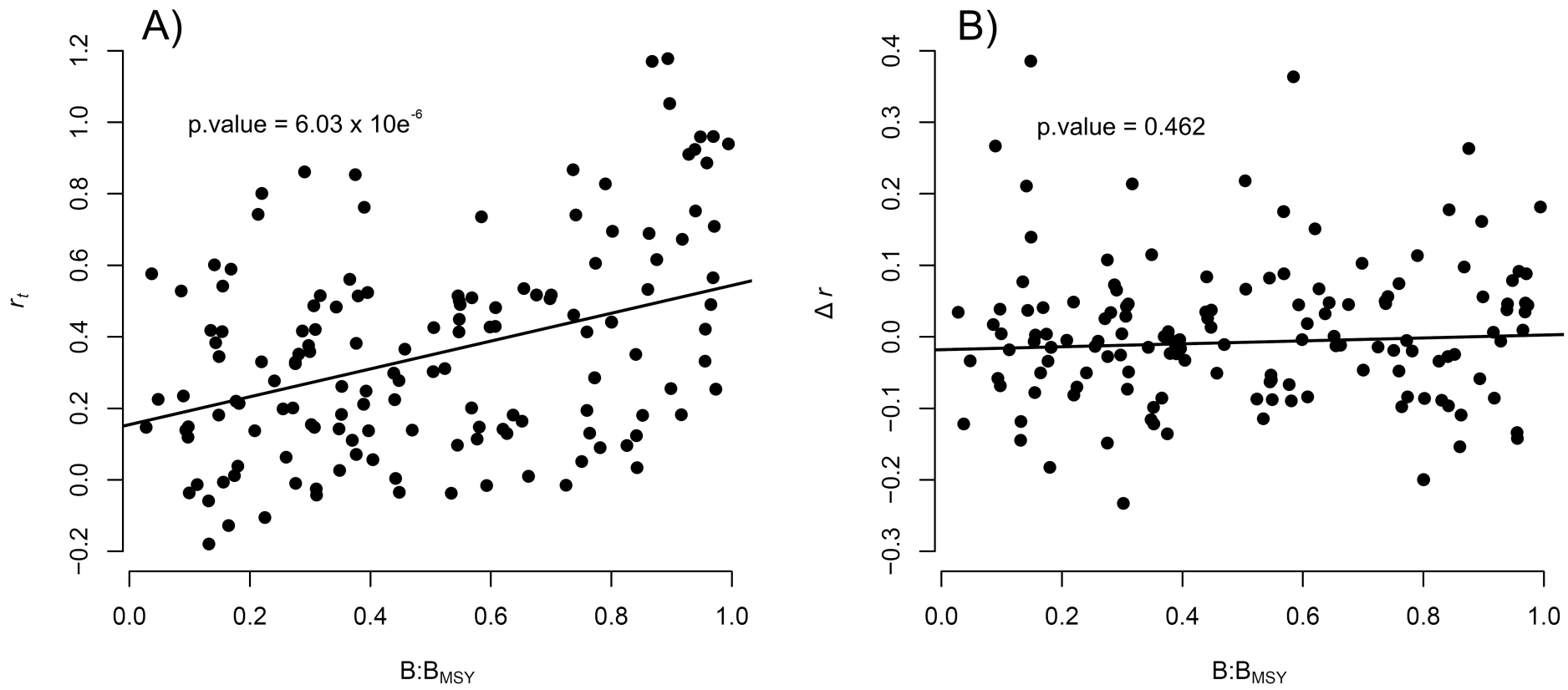

Figure 3.3. Relationship between contemporary productivity and stock status. (A) Gives the relationship between contemporary intrinsic productivity (estimated as the mode of r over the last five years) versus the mean ratio of estimated B to B_{MSY}, denoted $B:B_{MSY}$. Panel (B) gives the mode of the mean annual rate of change in r_t, denoted Δr , versus $B:B_{MSY}$.

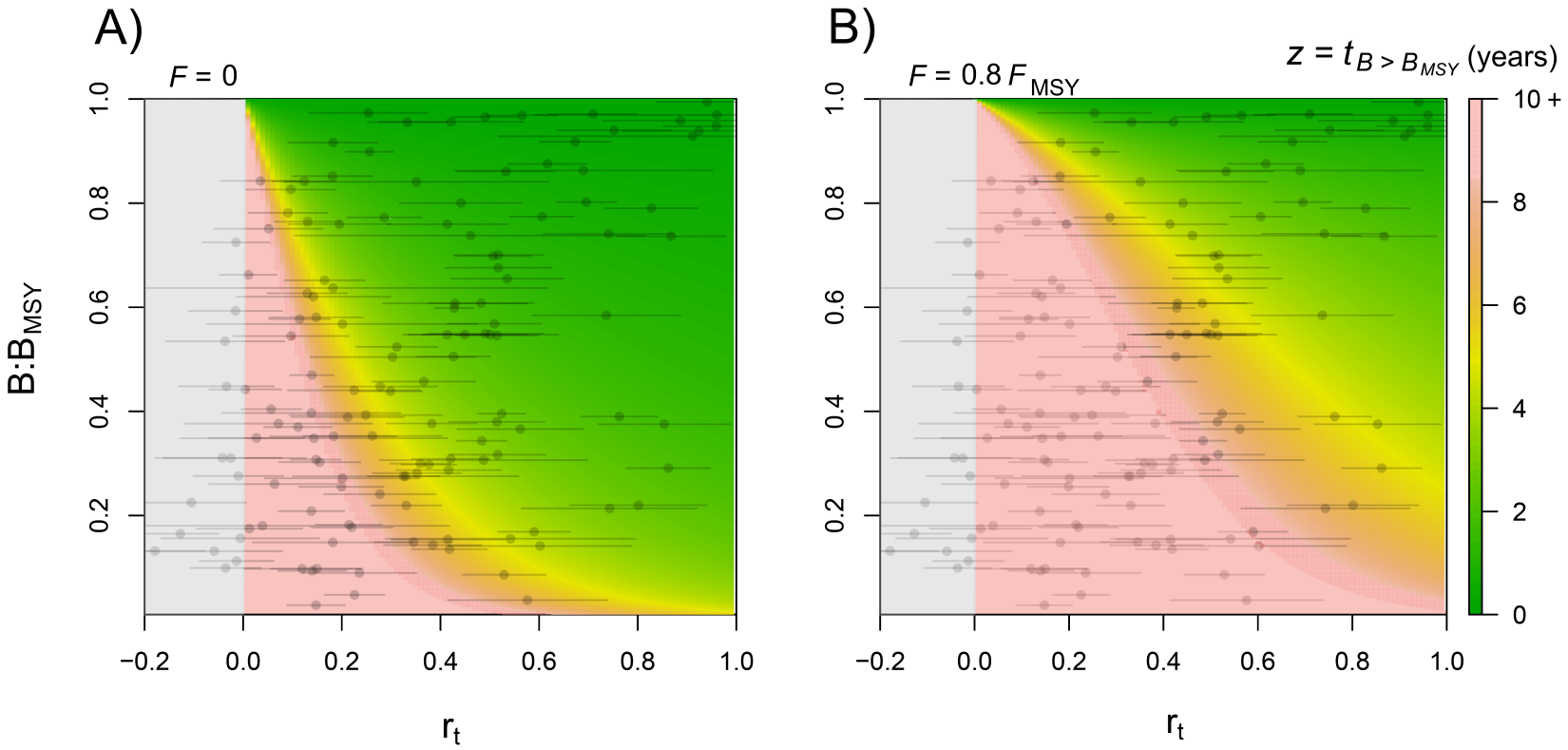

Figure 3.4. Rebuilding time as a function of contemporary productivity and stock status. (A) Predicted rebuilding time contours (in years t until B is greater than B_{MSY} when starting below) as a function of the ratio of current biomass B to target B_{MSY} under no fishing ($F = 0$). (B) Rebuilding contours when fishing pressure F is set at 80% of F_{MSY}. Contemporary stock status (mean $B:B_{MSY}$ for the most recent five years) and the estimated contemporary productivity with 95% credible interval (dot gives the mode, or most probable value) are superimposed for 133 depleted fish stocks. Populations in the grey-shaded areas have negative contemporary productivity and are not predicted to recover.

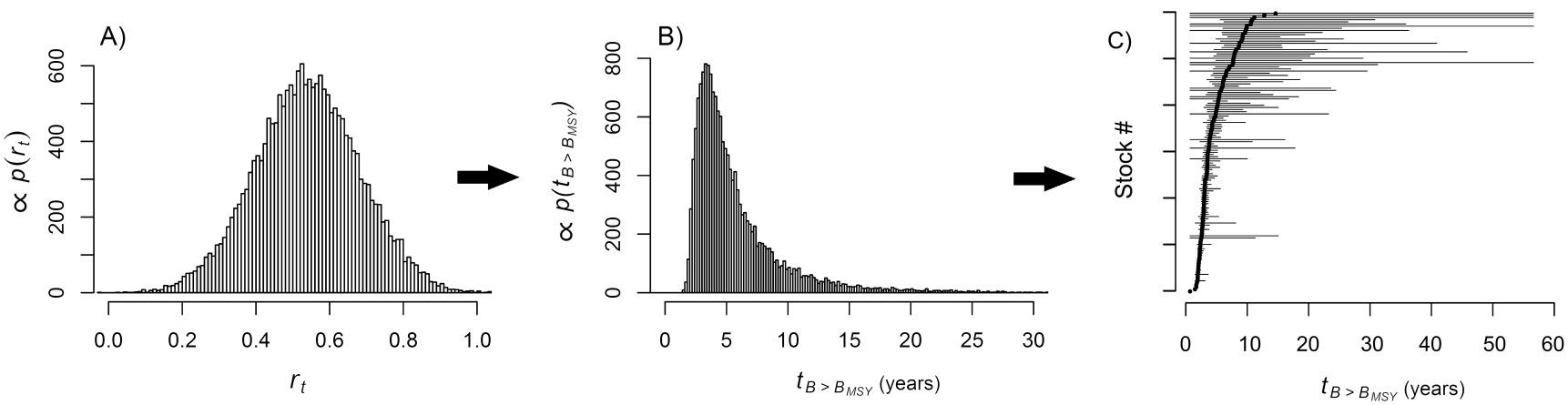

Figure 3.5. Skewed rebuilding time distribution under nonstationary productivity. When contemporary intrinsic productivity is described by a Gaussian probability distribution (A), the resulting rebuilding distribution is highly skewed due to the nonlinear dependence between rebuilding and productivity (B). Panel (C) gives the empirical rebuilding time distributions for 133 fish stocks currently below B_{MSY}. Note the characteristic strong positive skew.

Chapter 4

Discussion

Adapting to global climate change represents a key societal challenge for the 21st century. A major component of this effort is understanding and managing the impacts on the dynamics and productivity of our biological resources. I have attempted to address nonstationary productivity in global fish stocks by formulating and applying nonstationary extensions of two canonical productivity models at the regional, taxonomic, and global scales. The work was synthetic by integrating well-understood statistical tools with classic population models and applying them to a new and publicly available global database of fisheries time series. In Chapter 2, I evaluated nonstationary productivity in juvenile recruitment and demonstrated that recruitment capacity is declining in the majority of stocks and regions. These patterns were regionally coherent at the ecosystem level and were significantly linked to changes in the environment; specifically, temperature, phytoplankton, along with the degree of historical overfishing. In Chapter 3, I combined recruitment, growth, and natural mortality to focus on total productivity. I showed significant variability at the stock level and quantified the impacts for rebuilding timelines of depleted stocks. The results have informed the historical and contemporary status of fish stock productivity, revealed key environmental drivers, and have provided critical management feedback for understanding rebuilding potential in contemporary stocks.

Here I will attempt to highlight the salient implications of this work, focusing on follow-up research. I discuss two primary topics. The first concerns disparate trends between declining recruitment and more stable total productivity. This apparent inconsistency implies a 'missing ingredient' in our understanding of global fisheries ecology. I

discuss the relevant hypotheses and suggest research to test them empirically. Secondly, I discuss the implications of nonstationary productivity for adaptive and ecosystem-based fisheries management - first suggesting continued research into adaptive single species methods and then highlighting the prospects for integrating empirically-based adaptive strategies within a fully ecosystem-based fisheries management (EBFM) paradigm.

4.1 Productivity, recruitment, mortality, and growth

Throughout the thesis I have assumed that total productivity is the product of juvenile recruitment (no. of individuals produced by the spawning stock), individual growth (the accumulation of individual biomass), and integrated survivorship. Therefore declining patterns of recruitment observed in Chapter 2 would imply declining productivity, if other processes remain constant. However, results from Chapters 2 & 3 showed that long term trends in total productivity were remarkably flat when compared to recruitment. There are only a number of possible explanatory hypotheses:

1. Either growth or mortality (or both) have compensated for declining recruitment, resulting in relatively flat long term total productivity.

2. Declines in recruitment capacity are lagged relative to total productivity, meaning that the declines in recruitment will affect productivity in the future.

3. Stationary assumptions in the stock assessments leads to biomass estimates that tend to be more constrained toward constant total productivity, while recruitment is more empirically free to vary.

All three are very interesting and warrant further investigation. Hypothesis 1 should be readily testable with growth and mortality data. These data are often collected and analyzed within stock assessments but are not readily included in the RAM Legacy Stock

Assessment Database. I previously began extracting raw weight-at-age and abundance-at-age tables from the assessment documents but this proved complicated and outside the scope of my research. Based on preliminary analyses, most trends in growth appeared negative but further data synthesis and analysis are required to properly test the hypothesis. This should be a priority for follow-up research.

The ultimate test of hypothesis 2 is time. However it may also be testable in the interim by correlating trends at more local scales. The trend estimates reported in Chapters 2 & 3 were calculated on a *multidecadal scale*, therefore my results only imply that long term trends in recruitment capacity were stronger than long term trends in total productivity. It is possible that there have been more recent trends in productivity which correlate with more recent trends in recruitment. This is a relatively straightforward extension of the work presented here and should be followed up in the short term.

Hypothesis 3 is more difficult to address. The general problem of 'assessment bias' was raised by Walters [20] but he gave no reason to believe that recruitment or total productivity would be any more or less prone to this problem. However, the distinction was raised by an experienced stock assessment scientist [59] who pointed to a possible explanation by way of subjective management decisions made within the assessments. Specifically, one often sums contributions from biomass, recruitment, and growth when minimizing a cost function to fit an assessment model. Due to management constraints, there can be a subjective tendency to up-weight biomass deviations and down-weight recruitment within the cost function [59] resulting in biomass estimates which more closely resemble the deterministic model solution, relative to recruitment. This is a difficult hypothesis to test based on available information [25] but has potentially serious implications for management. If such a situation were true, the observation of declining recruitment may point to declining productivity which remains clouded in the assessments due to to inherent stationarity assumptions in the assessment models. This highlights the need to integrate nonstationary methods directly into the assessment models in order to diagnose

nonstationary processes from raw survey-based fisheries data.

Another important question concerns the environmental drivers of total productivity. In Chapter 2 I related nonstationary recruitment capacity to trends in ocean temperature and phytoplankton abundance. But in Chapter 3 I focused on management consequences of total productivity and did not explore potential relationships with environmental variables. I do note, however that recruitment capacity displayed much higher variation at the regional level which suggested a stronger environmental signal. Total productivity was more regionally static so the environmental signal is likely weaker; however this should be followed up with statistical analyses.

4.2 Adaptive ecosystem-based fisheries management

Here I discuss the implications of nonstationary processes for adaptive ecosystem-based fisheries management. I first discuss *adaptive* and *ecosystem-based* separately, and then I discuss the possibility of integrating adaptive Bayesian methods within a fully ecosystem-based approach.

Regarding adaptive management strategies, this work has focused on how to adapt quantitative biological parameters in the light of single-species time series; however there remains a critical question of how to adapt management and optimal harvest strategies in response to nonstationary productivity. In my view, there are two considerations:

1. How does annual F relate to optimal long term maximum sustainable yield in the context of nonstationary resources? It is unlikely that matching annual F to time-varying F_{MSY} achieves this goal, due to the fact that F_{MSY} is optimized with respect to population equilibrium [55]. However this is a testable theoretical question.

2. How does one maximize long term sustainable yield of nonstationary resources in the context are *socioeconomic constraints*? The allocation of individual licenses and annual quota may impose a constraint whereby fishing effort can only be changed

slowly to maintain a sustainable employment environment. Based on the socioeconomics of individual fisheries, managers may then impose a *maximum tolerable flexibility* within which it is acceptable to adjust quota in response to annual productivity predictions. This is another constraint to consider in the optimization of long term yield with respect to nonstationary resources.

Regarding ecosystem-based fisheries management (EBFM), the adaptive single-species methods used in this thesis do not explicitly model ecosystem processes. True EBFM is predicated on modelling the ecosystem directly including 'end-to-end' relationships with fish stock productivity [9, 60]. While there is significant practical disagreement regarding the appropriate implementation of EBFM [57, 61], there is clear tension between the tractability of single-species models and ecosystem complexity [62]. Furthermore, calibrating ecosystem-scale models with historical data runs the same risks identified by Walters [20] whereby critical ecosystem properties are nonstationary and challenge the appropriateness of parameters calibrated with historical data. Excitingly, however, ecosystem-scale models based on empirical Bayesian updating are already coming online [63–66]. In such models, dynamic biological parameters are modelled in the lower trophic levels and updated on account of sophisticated oceanographic observations. The act of sequentially conditioning on new observations provides a full probabilistic *online* description of the ecosystem state. The next logical step is integrate end-to-end models (e.g. [60, 67]) with Bayesian updating to make probabilistic online predictions of stock stock productivity based on ecosystem conditions. By constraining ecosystem complexity in an empirical and probabilistic way, these methods are ripe to form the basis of 21$^{\text{st}}$ century ecosystem-based fisheries management and will only become more powerful with novel observing platforms and advanced computational tools.

4.3 Conclusions

In conclusion, it is becoming increasingly clear that fisheries are responding to their changing environment. Therefore, our management of fish stocks must increasingly observe and adapt to nonstationary ecological conditions. Results in Chapters 2 & 3 have identified key environmental drivers, regional priorities, and management implications for depleted populations. I have also highlighted an empirical tool for understanding such processes through nonstationary extensions of classical biological models using sequential Bayesian updating. The situation is neatly summarized by well-known engineering paradigm, *one can't manage what one doesn't measure*. Indeed it is not until we measure ecological change that we can break ourselves from the dangerous assumption that the future will resemble the past. Only then can we speak of *sustainable fisheries managment*. I hope these results have furthered that effort.

Appendices

Appendix A

Methods for Chapter 1

Environmental change drivers declining recruitment capacity in global fish stocks

A.1 Data

The stock-recruitment data were extracted from the RAM Legacy Stock Assessment Database [25]. This is a global, quality controlled database, available publically at http://ramlegacy.marinebiodiversity.ca/. Stock assessments provide estimates of both spawning stock biomass (kg) and recruitment (no. individuals). We analyzed 262 of the 420 time series available in the database. This subset was chosen according to: 1) The abundance time series must be estimated via Virtual Population Analysis (VPA) or another stock assessment model that does not use a deterministic recruitment function in estimating stock and recruitment abundances; and 2) the spawning stock biomass and recruitment time series must be estimated directly, as opposed to those based on indirect proxies such as spawner egg abundance. All series were then normalized to unit variance for easy comparison across stocks and regions. A list of species used in the analysis, along with their designated LME can be found in Table A.1.

A.2 State space model parameterization

The Ricker model can be linearized by re-expressing recruitment as log survival

$$\log\left(\frac{R_t}{B_{t-\tau}}\right) = \log\alpha - \beta B_{t-\tau}.$$

This model can be fitted to data as a linear regression which is made explicit by setting $\mathbf{y} = \log \frac{R_t}{B_{t-\tau}}, \theta_0 = \log \alpha$, and $\theta_1 = \beta$. In matrix notation we write the linear regression model

$$\mathbf{y} = [\mathbf{1}, \mathbf{B_{t-\tau}}] \begin{bmatrix} \theta_0, \\ \theta_1 \end{bmatrix} + \mathbf{e} = \mathbf{H}\theta + \mathbf{e},$$

where $\mathbf{e}$ is a normally distributed random error vector with zero-mean and covariance Σ, and $\mathbf{H}$ is the Tx2 design matrix of the regression model (where T is the length of the time series) with a vector of ones on the first column and the observed spawning stock biomass $\mathbf{B_{t-\tau}}$ as the right column.

To model nonstationary recruitment, we let the recruitment parameters θ vary in time, yielding a dynamic linear regression, which is a special case of a linear Gaussian state space model (a.k.a. dynamic linear model)

$$\begin{aligned} y_t &= \mathbf{H}_t\theta_t + w_t & w_t &\sim N(0, \mathbf{R} = \sigma_o^2), \\ \theta_t &= \theta_{t-1} + v_t & v_t &\sim N\left(\mathbf{0}, \mathbf{Q} = \begin{bmatrix} \sigma_{\theta_0}^2 & 0 \\ 0 & \sigma_{\theta_0}^2 \end{bmatrix}\right), \end{aligned}$$

where y_t is the observed log survival at time t, w_t is a realization of the Gaussian observation error at time t with variance $\mathbf{R}$, and v_t is a realization of the bivariate Gaussian process error at time t with covariance $\mathbf{Q}$. Given numerical parameter values for $\mathbf{R}$ and $\mathbf{Q}$, along with the initial value distribution (or prior distribution) for the recruitment parameters, denoted $\theta_\mathbf{0}$, the optimal reconstruction for the latent time-varying recruitment parameters $\theta_\mathbf{t}$ are estimated using the Kalman filter and smoother. For clarity, we make

the distinction between variance parameters ($\mathbf{R}$ and $\mathbf{Q}$) which need to be estimated by maximum likelihood, and recruitment parameters ($\theta_\mathbf{t}$) which are analytically determined by the Kalman filter/smoother algorithm, conditional on $\mathbf{R}$, $\mathbf{Q}$, and $\theta_\mathbf{0}$.

A.3 State space model estimation

The algorithm above assumes that the variance parameters are known; but for a given time series we estimate the variance parameters by Maximum Likelihood Estimation (MLE) which is based on the normally distributed one-step ahead prediction errors of the filtering algorithm, termed the innovations. The innovations for the dynamic regression are given by

$$\delta_t = y_t - \mathbf{H}_t \hat{\theta}_{t|t-1}.$$

The error covariance of the innovations is defined by

$$\mathbf{F}_t = \mathbf{H}_t \mathbf{M}_t \mathbf{H'}_t + \mathbf{R}.$$

The log likelihood of the innovations can then be written down as

$$\log L(\mathbf{R}, \mathbf{Q}) = c - \frac{1}{2} \sum_{t=1}^{T} \log |\mathbf{F}_t| - \frac{1}{2} \sum_{t=1}^{T} \delta'_t \mathbf{F}_t \delta_t,$$

and maximized using standard nonlinear optimization, yielding MLE estimates of $\mathbf{R}$, $\mathbf{Q}$, and subsequently $\theta_{t|N}$ by applying the Kalman smoother algorithm. All calculations were written in the R language (www.r-project.org) and the optimization was performed using the numerical routines within the R base package.

A.4 Model Selection

To determine whether individual recruitment time series have stationary or nonstationary parameters, we applied model selection using various parameterizations of the matrix $\mathbf{Q}$. We used the Bayesian Information Criterion (BIC) for model selection which is given as

$$\text{BIC} = -2 \log \hat{L} + k \log T,$$

where $\log \hat{L}$ is the optimized value of the log likelihood, k is number of nonzero estimable variance parameters in the dynamic regression model, and T is the length (number of years) of an individual recruitment time series. We consider four parameterizations of $\mathbf{Q}$ which represent: 1) static stock-recruit relationship (all elements of $\mathbf{Q}$ equal to zero; $k = 1$); 2) time-varying maximum reproductive rate, static density-dependence ($\mathbf{Q}_{[1,1]} \neq 0$, all others zero; $k = 2$); 3) static maximum reproductive rate, time-varying density-dependence ($\mathbf{Q}_{[2,2]} \neq 0$, all other zero; $k = 2$); 4) time-varying maximum reproductive rate and density-dependence ($\{\mathbf{Q}_{[1,1]}, \mathbf{Q}_{[2,2]}\} \neq 0$, all others zero; $k = 3$). Under each parameterization, the Kalman filter/smoother algorithm yields a likelihood which is optimized to compute the BIC. (Note that we adopt the BIC over the more common Akakie Information Criterion (AIC) to be more conservative in model selection in the sense that BIC favors fewer parameters due to its stricter penalty term (i.e. for $n \geq 8$, the BIC penalty $k \ln n$ is greater than the AIC penalty $2k$) and will thus discriminate more strongly against time-varying recruitment parameters).

A.5 Post-hoc trend estimation

The dynamic linear regression analysis yields $\theta_{t|N}$ for 262 fish populations. For an individual stock i we use $\theta^i_{t|N}$ to calculate $R^i_{MAX}(t)$ and then summarize the trend using a linear

slope based on generalized least squares regression in order to account for autocorrelation

$$R^i_{MAX}(t) = b^i_0 + b^i_1 t + e^i_t,$$

where b^i_0 is the intercept of the linear regression for stock i, b^i_1 is the slope multiplied by time index t, and e^i_t is the regression error at time t with covariance Σ. To standardize the rate of change in recruitment and avoid excessive decimal places, we define

$$\Delta R^i_{MAX} = \frac{b^i_1}{\max(R^i_{MAX}(t))} * 10 \text{ years},$$

which represents the rate per decade (10 years) as a percent relative the historical maximum of R^i_{MAX}.

To estimate the uncertainty in ΔR^i_{MAX} according to the uncertainty in the estimated time-evolving recruitment parameters, we use a resampling scheme as follows.

Resample Linear Slope:

$for\ j = 1, 2, \ldots, 500$

1. Sample a time sequence from smoother distribution: $\theta^{i,j}_{t|N} \sim N(\theta^i_{t|N}, P_{t|N}))$.
2. Compute $R^{i,j}_{MAX}(t)$ as a function of $\theta^{i,j}_{t|N}$.
3. Estimate the regression coefficients of $R^{i,j}_{MAX}(t) = b^{i,j}_0 + b^{i,j}_1 t + e^{i,j}_t$ using least squares.
4. Compute $\Delta R^{i,j}_{MAX} = \frac{b^{i,j}_1}{\max(R^{i,j}_{MAX}(t))} * 10$.

This procedure yields bootstrapped distributions of ΔR^i_{MAX} for use in the subsequent

analyses. This scheme was adopted for the specific purpose of propagating the uncertainty in $\theta_{t|N}$, opposed to simply taking the standard error on the least squares regression which would assume $\theta_{t|N}$ known and fixed. Due to the nonlinearity in $R_{MAX}(t)$ we use the median and median absolute deviation (MAD) as summary statistics for robustness.

A.6 Meta-analysis

To combine the results of the individual trend analyses, we perform a random-effects meta-analysis at the taxonomic, regional, and global scales. For any particular grouping k of $i = 1, 2, , N_k$ stocks (i.e. taxonomic, regional, or global), the random-effects model is written

$$\Delta R^i_{MAX} = \Delta R^k_{MAX} + \xi^i + \psi^i,$$

where ΔR^i_{MAX} is the estimated linear slope of R_{MAX} for stock i, ΔR^k_{MAX} is the overall mean ΔR_{MAX} for the N stocks in group k, ξ^i is the deviation of the observed ΔR^i_{MAX} from the true ΔR^i_{MAX}, and ψ^i is the deviation of the true ΔR^i_{MAX} from ΔR^k_{MAX}. In the estimation, weights are applied according to the inverse variance of the bootstrap distribution of ΔR^i_{MAX}. The meta-analysis model was implemented in the R package *rmeta* [68].

A.7 Drivers of ΔR^k_{MAX}

We related the LME-specific ΔR^k_{MAX} values to LME-specific environmental and fisheries-related variables including linear trends in sea surface temperature (ΔSST spanning 1957-2006), chlorophyll concentration (ΔCHL a widely-used proxy for phytoplankton biomass; 1899-2010), and an index of historical overfishing, taken as the mean historical ratio of

annual biomass to target biomass levels ($\mathrm{B{:}B_{MSY}}$) as extracted from the stock assessments [25]. We perform a multiple regression of the form

$$\Delta R^k_{MAX} = c_0 + c_1 \Delta\mathrm{SST} + c_2 \Delta\mathrm{CHL} + c_3 \mathrm{B{:}B_{MSY}} + e_k,$$

where ΔR^k_{MAX} is the meta-analytic mean estimated per LME k containing (each containing a different number of stocks), e_k is the LME-specific regression error, and the constants denoted c_i where $i = \{0, 1, 2, 3\}$ are the partial regression coefficients. The regression was weighted according to the number of stocks in each LME. The best fitting variables were chosen according to BIC model selection. We tested two interactions between ΔSST and $\mathrm{B{:}B_{MSY}}$, and ΔCHL and $\mathrm{B{:}B_{MSY}}$, but neither were retained in model selection. We also tested for spatial correlation but it was not favored based on BIC. All independent variables were standardized to unit variance in order to standardize the regression coefficients. Pairwise scatterplots of the environmental variables are plotted in Figure A.5 and indicate negligible colinearity.

The multiple regression analysis was performed three times on three sets of species. The first included all species with each LME. Secondly and thirdly, we took two subsets of the species within each LME according to their taxonomic order. One taxonomic grouping included *Gadiformes* and *Pleuronectiformes* and the other included *Clupeiformes* and *Perciformes*. These orders do not occur in all LMEs, therefore the regression analysis on the subsets included a limited number of species. The *Gadiformes* and *Pleuronectiformes* occurred in 21 LMEs and the *Perciformes* and *Clupeiformes* occurred in 23 LMEs.

A.8 Analysis of Recruitment since the year 2000

In order to diagnose more recent changes in recruitment, we repeated the meta-analysis and environmental regression analysis using time-varying recruitment parameters, stock

biomass, and temperature since the year 2000. This was done through the following steps:

1. We first calculated all single-stock bootstrapped linear slopes using time-varying recruitment parameters since 2000 only.

2. We then performed the regional meta-analysis on the single-species species slopes to obtain the regional slopes for the period since 2000.

3. We calculated SST and B:B_{MSY} since 2000 (note that ΔCHL did not change here because we already used linear slope estimates from Boyce et al. 2014 [29], therefore the estimated rate of change is constant since 1890).

4. We performed the regional multiple regression on the basis of variables calculated since 2000.

A.9 Basic R code

```
##############################################################################
##############################################################################
## ------------------------------------------------------------------------ ##
## This code represents the likelihood function for the Kalman filter  ##
## It computes the hidden states of a linear Gaussian state space model##
## \\ as a function of the variance parameters ---------------------- ##
## \\ and evaluates the likelihood ---------------------------------- ##
## This function is numerically optimized ---------------------------- ##
## \\ to give the Maximum Likelihood Estimates for the variances ----- ##
## ------------------------------------------------------------------------ ##
##############################################################################
##############################################################################

kallike <- function(theta)

{
  D <- matrix(c(1,0,0,1),ncol=2)
  ID <- matrix(0,ncol=2,nrow=2)
  diag(ID) <- 1

  ones <- rep(1,T)
  H <- cbind(ones,ssb)
  xf <- matrix(0,2,T)
  x <- matrix(0,2,T)
  Ppreds <- array(0,dim=c(T,2,2))
  P <- array(0,dim=c(T,2,2))
```

```
  F <- matrix(0,nrow=T)
  v <- numeric(T)

  R <- exp(theta[1])

  sig.i <- 1e+7
  P[1,1,1] <- P[1,2,2] <- sqrt(sig.i)

for(k in 1:(T-1))
{
  xold <- matrix(x[,k])
  Pold <- P[k,,]

  xfnew <- D%*%xold
  Ppred <- D%*%Pold%*%t(D)+Q
  xf[,k+1] <- matrix(xfnew)
  Ppreds[k+1,,] <- Ppred

  yobs <- matrix(y[k+1])
  Fnew <- H[k+1,]%*%Ppred%*%matrix(H[k+1,])+R
  K <- Ppred%*%matrix(H[k+1,])%*%pseudoinverse(Fnew)
  xnew <- xfnew+K%*%(yobs-(H[k+1,])%*%xfnew)
  Pnew <- (ID-(K%*%H[k+1,]))%*%Ppred

  x[,k+1] <- xnew
  P[k+1,,] <- Pnew
  F[k+1] <- Fnew
  v[k+1] <- (yobs-(H[k+1,])%*%xfnew)
}

L <- 0

for(k in 2:T)
{
  F1 <- as.matrix(F[k])
  L <- L-T/2*log(2*pi)-1/2*log(det(matrix(F1)))
         \\ -1/2*t(v[k])%*%pseudoinverse(F1)%*%v[k]
}

return(-L)
}
```

A.10 Appendix Figures

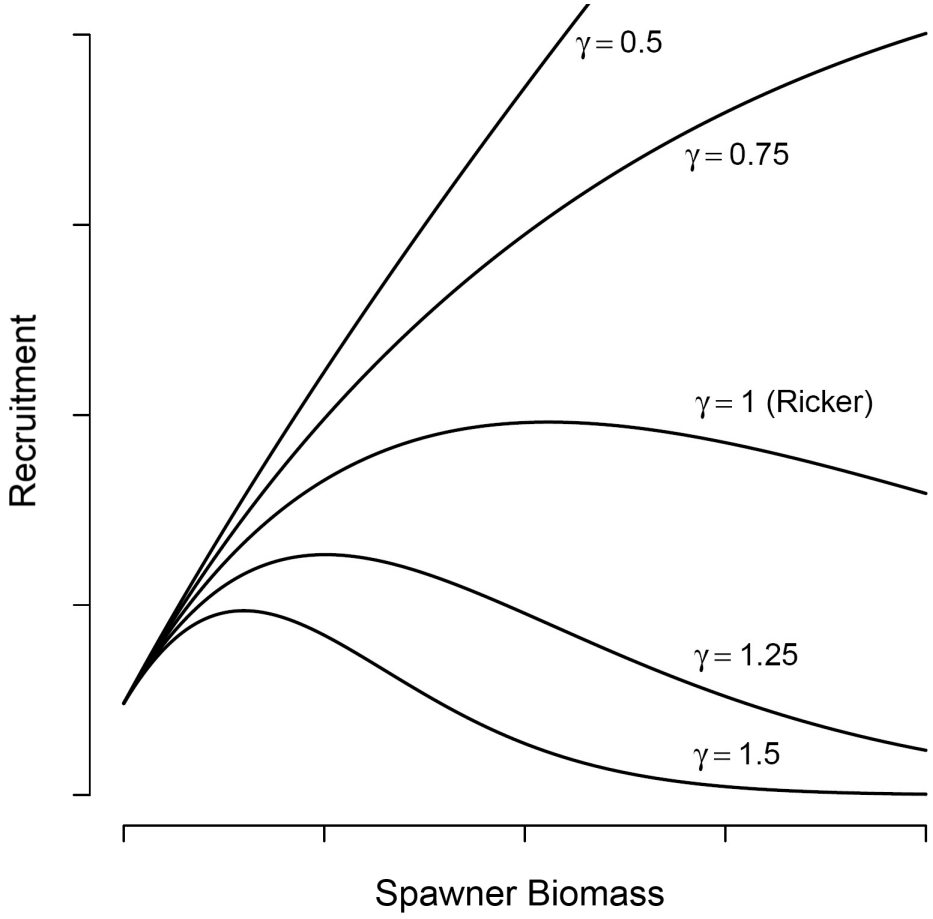

Figure A.1. The generalized Ricker model and alternate forms of density-dependence. The shape parameter γ in the generalized Ricker model has a strong effect on the form of density-dependence in the stock-recruit relationship. Increasing values of γ lead to stronger density-dependence feedback, and as $\gamma \to 0$ the generalized Ricker describes a linear relation between stock and recruitment with slope α.

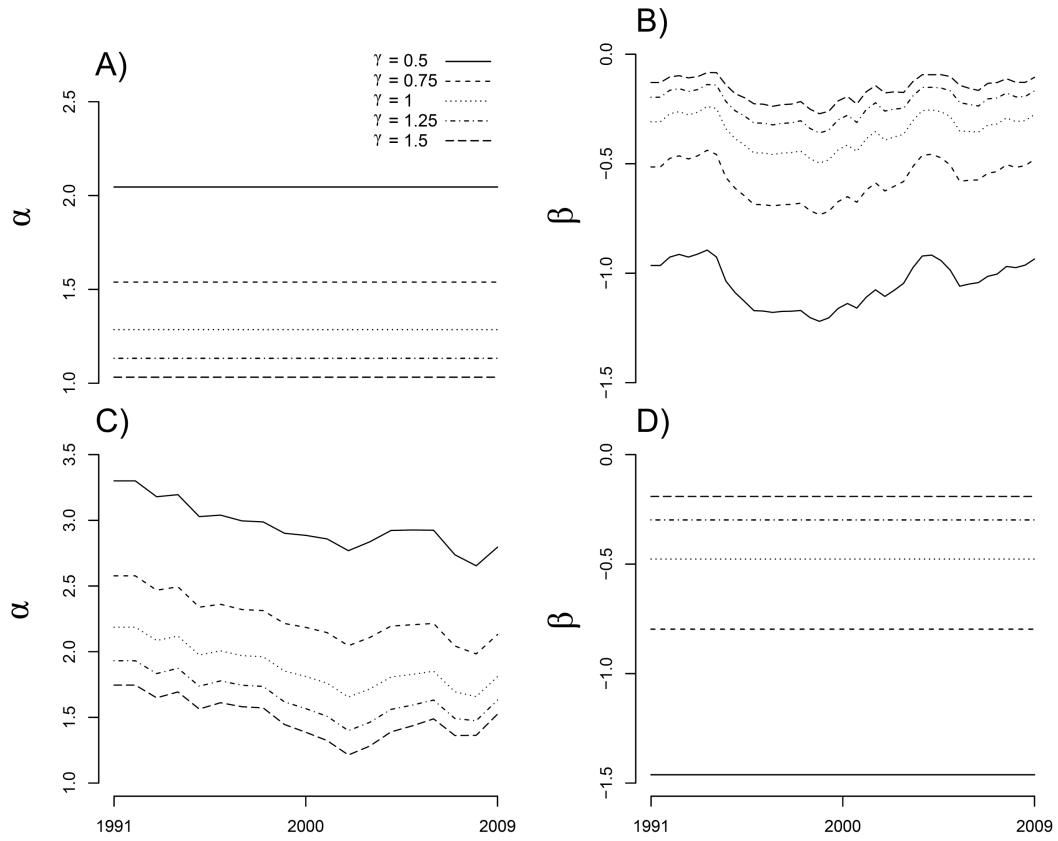

Figure A.2. Effect of γ transformation on recruitment parameters α and β. As examples, Panels A and B give the estimated recruitment parameters for Peruvian anchoveta (North-Central Peru) and Panels C and D give recruitment parameters for Southern blue whiting (Southern Argentina). The two stocks exhibited time-varying α and β, respectively, according to model selection. The reader should note that varying γ affects the magnitude of the parameters, but not the time-variability. As a result, the standardized slopes (when expressed in terms of % relative to historical maximum) remain constant and independent of γ.

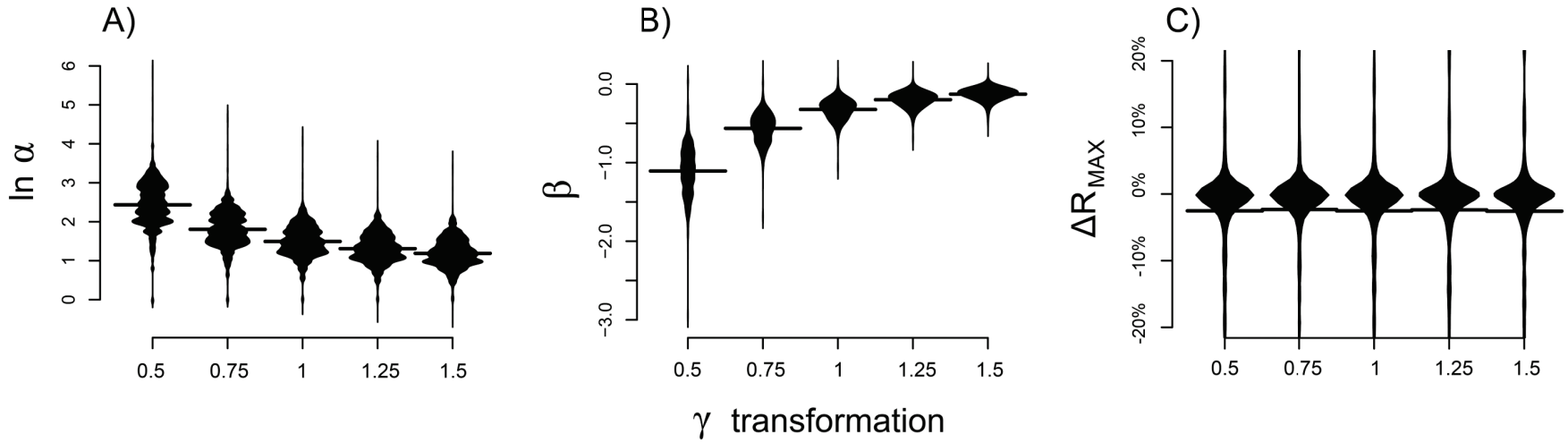

Figure A.3. Sensitivity analysis. To test the sensitivity of ΔR_{MAX} to alternate forms of the stock-recruit relationship, the dynamic regression models were applied to the generalized Ricker model using prescribed values for the shape parameter γ (see Figures A.1 and A.2). Panels A and B give the distribution and median of α and β estimates under each value of γ (note $\gamma = 1$ recovers the traditional Ricker model used in this study) and Panel C gives the distribution of the standardized linear slopes ΔR_{MAX} under the γ transformations. These results imply that the ΔR_{MAX} quantity (when expressed in terms of % relative to historical maximum) was independent of the form of density-dependence in the generalized Ricker model.

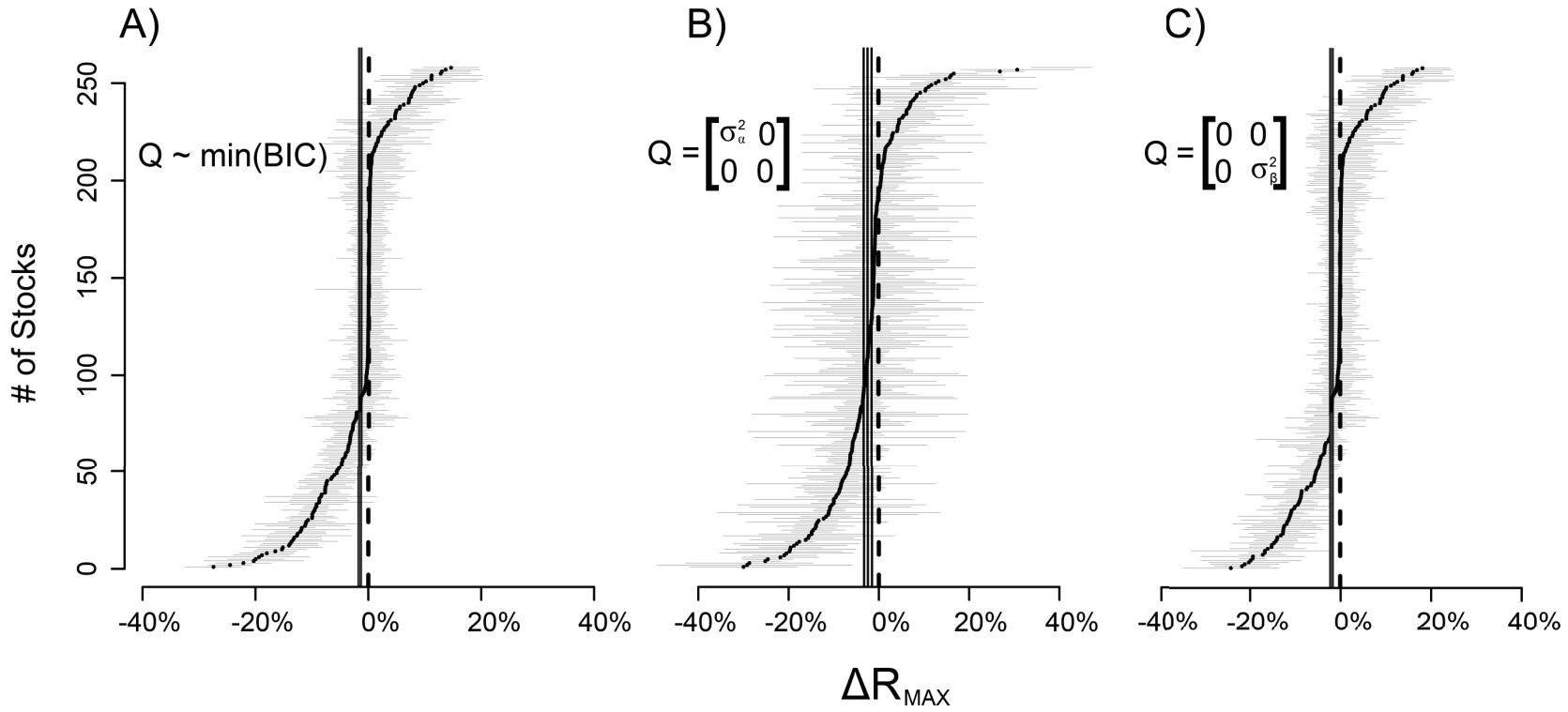

Figure A.4. Sensitivity of ΔR_{MAX} to model selection and specification. We tested the sensitivity of individual ΔR_{MAX} to the parameterization of the covariance matrix of the recruitment parameters $\mathbf{Q}$. Panel A gives the distribution of ΔR_{MAX} (and standard error) when choosing the elements of $\mathbf{Q}$ according to BIC model selection. Panel B gives the distribution ΔR_{MAX} when performing model selection between static stock-recruit vs. time-varying α, and Panel C gives ΔR_{MAX} for model selection between static stock-recruit and time-varying β. These results imply that maximum recruitment potential was relatively independent of whether we allowed α or β to vary.

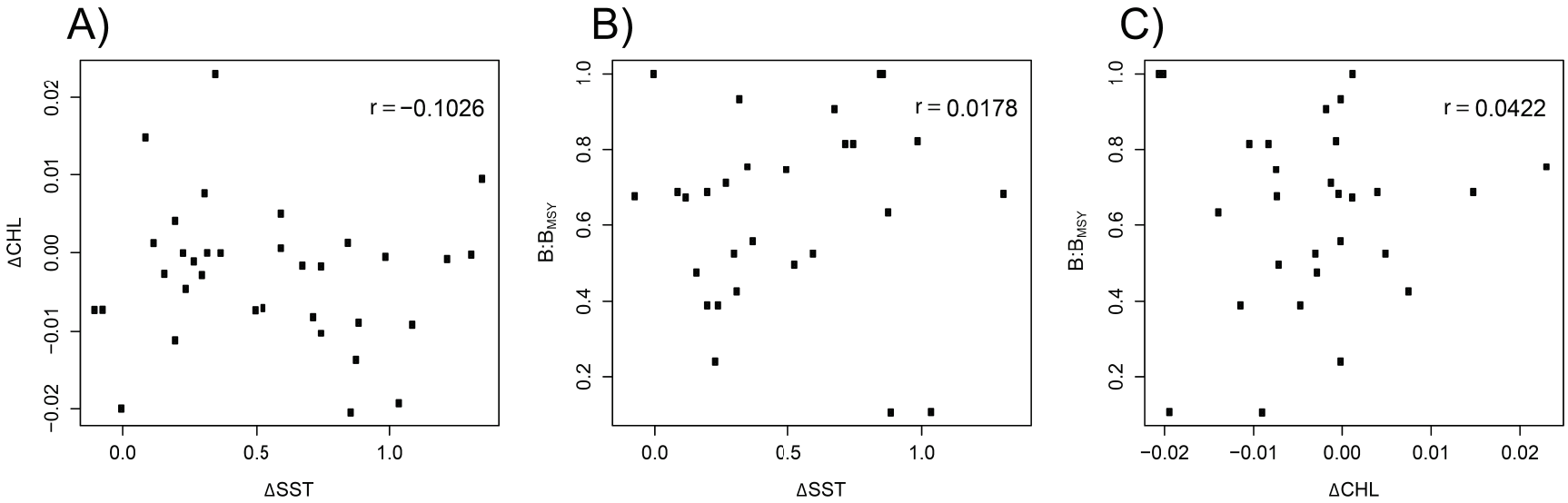

Figure A.5. Covariation in environmental and fishing related variables used in the multiple regression analysis of LMEs. Each point represents an LME and the value of the Pearson correlation coefficient is labelled in the corner of each plot. Scatterplots indicate negligible colinearity.

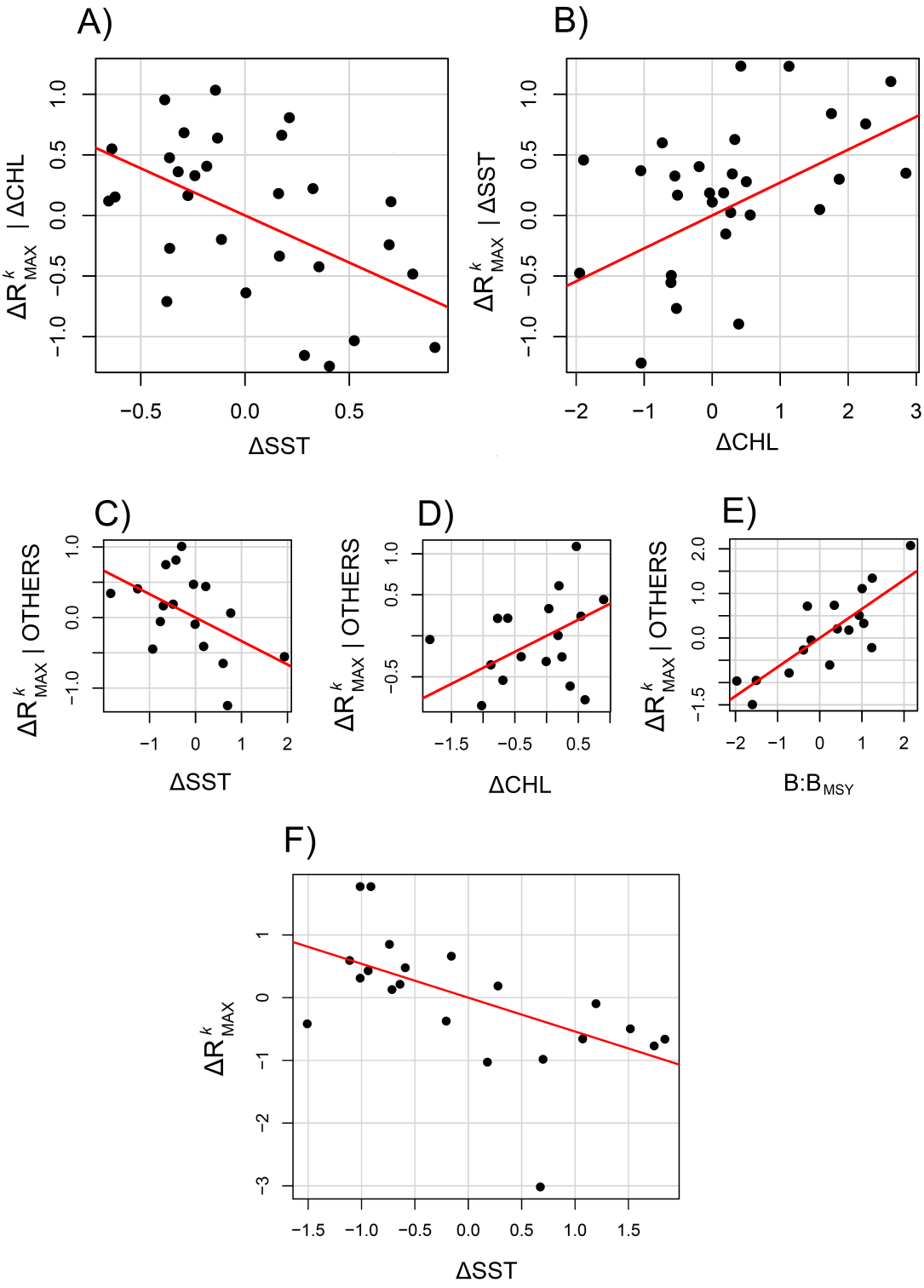

Figure A.6. Partial regressions of LME-specifc ΔR^k_{MAX} (representing ΔR_{MAX} at the LME level) against three potential drivers, ΔSST, ΔCHL, and B:B$_{\mathbf{MSY}}$. Panels A and B represents all taxa, Panels C-E represent orders *Gadiformes* and *Pleuronectiformes*, and Panel F represents orders *Clupeiformes* and *Perciformes*. Plotted are LMEs with > 1 stock present. The notation $\Delta R^k_{MAX}|X$, where X is an independent variable, represents the residuals of ΔR^k_{MAX} after being regressed against X.

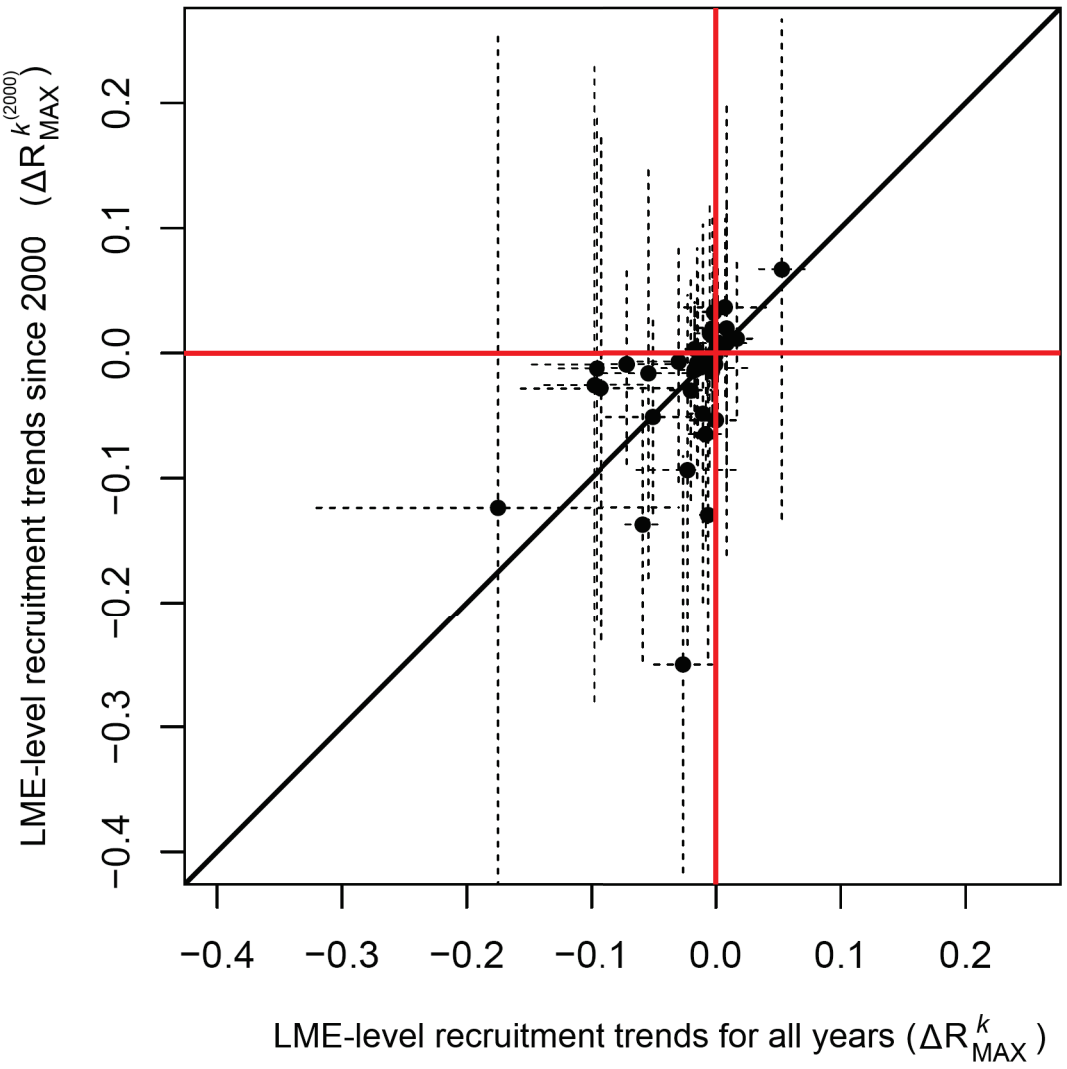

Figure A.7. Relationship between ΔR^k_{MAX} over two time periods. On the x axis is ΔR^k_{MAX} when calculated using all years in the stock assessments (as reported in the paper) and the y axis gives ΔR^k_{MAX} when using data since the year 2000 (y axis). Note the relatively high uncertainties in the y direction, yielding no significant departure from the black 1:1 line.

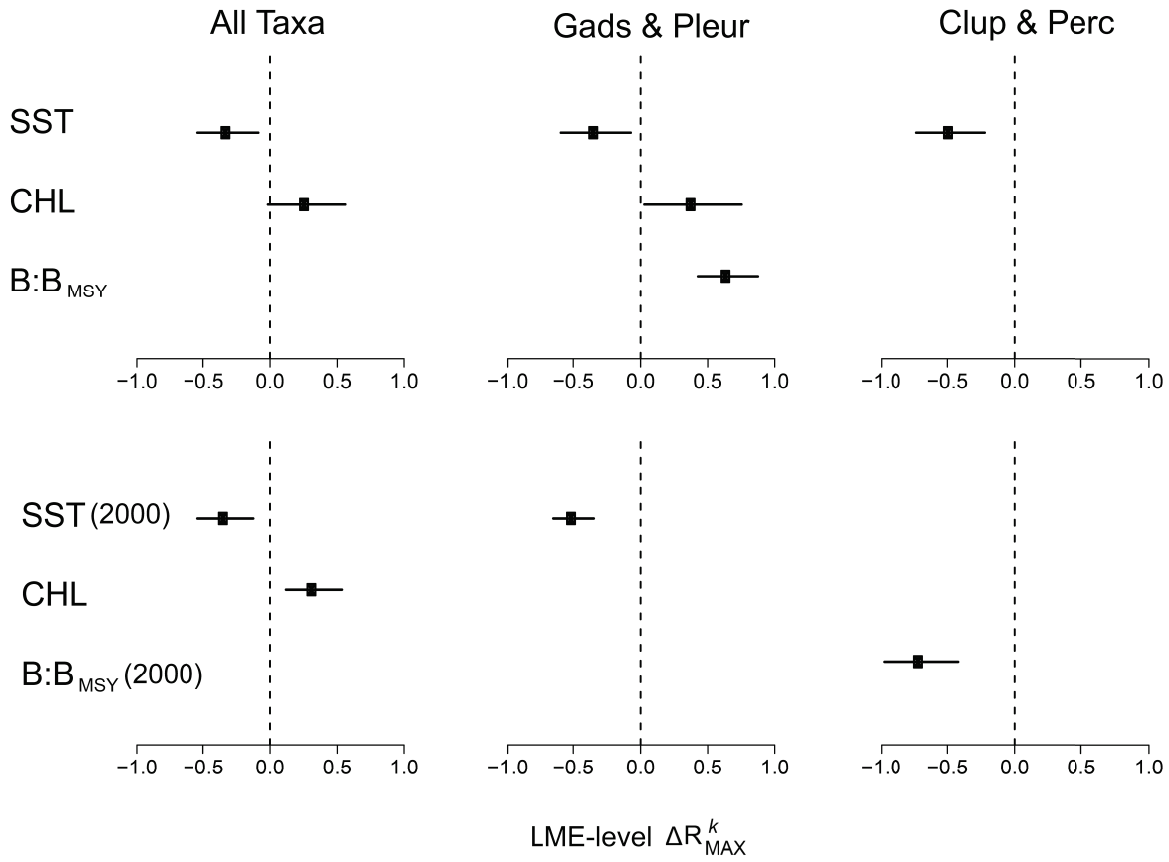

Figure A.8. Results from multiple regression analysis based on ΔR^k_{MAX} since 2000. The top row gives the results from the paper where all years in the stock assessments were used. The bottom row shows the relationship between ΔR^k_{MAX} since 2000 and ΔSST and B:B_{MSY} variables calculated since 2000 (note that the ΔCHL variable does not change over this period because the variable already represents a linear slope since 1899 [29]).

Table A.1. Stocks used in recruitment analysis

Common Stock ID [25]	**Large Marine Ecosystem**
Acadian redfish Gulf of Maine & Georges Bank	Northeast U.S. Continental Shelf
Alaska plaice Bering Sea and Aleutian Islands	East Bering Sea
Albacore tuna North Pacific	North Pacific ocean
Albacore tuna South Pacific Ocean	South Pacific ocean
American lobster Georges Bank	Northeast U.S. Continental Shelf
American lobster Gulf of Maine	Northeast U.S. Continental Shelf
American lobster Southern New England	Northeast U.S. Continental Shelf
American Plaice NAFO-23K	Newfoundland-Labrador Shelf
American Plaice NAFO-3LNO	Newfoundland-Labrador Shelf
American Plaice NAFO-3M	Newfoundland-Labrador Shelf
American Plaice NAFO-5YZ	Northeast U.S. Continental Shelf Scotian Shelf
Anchovy ICES VIII	Iberian Coastal
Anchovy kilka Caspian Sea	Black Sea
Anchovy South Africa	Benguela Current & Agulhas Current
Argentine anchoita Northern	Patagonian Shelf & South Brazil Shelf
Argentine anchoita Southern	Patagonian Shelf
Argentine hake Northern Argentina	Patagonian Shelf & South Brazil Shelf
Argentine hake Southern Argentina	Patagonian Shelf
Arrowtooth flounder Bering Sea and Aleutian Islands	East Bering Sea
Arrowtooth flounder Gulf of Alaska	Gulf of Alaska
Arrowtooth flounder Pacific Coast	Gulf of Alaska
Atka mackerel Bering Sea and Aleutian Islands	East Bering Sea
Atlantic butterfish Gulf of Maine & Cape Hatteras	Northeast U.S. Continental Shelf
Atlantic cod Baltic Areas 22 and 24	Baltic Sea
Atlantic cod Baltic Areas 25-32	Baltic Sea

Atlantic Cod Celtic Sea	Celtic-Biscay Shelf
Atlantic cod coastal Norway	Barents Sea & Norwegian Sea
Atlantic cod Faroe Plateau	Faroe Plateau
Atlantic cod Georges Bank	Northeast U.S. Continental Shelf
Atlantic cod Gulf of Maine	Northeast U.S. Continental Shelf
Atlantic cod Iceland	Iceland Shelf
Atlantic cod Irish Sea	Celtic-Biscay Shelf
Atlantic cod Kattegat	North Sea
Atlantic cod NAFO 2J3KL inshore	Newfoundland-Labrador Shelf
Atlantic cod NAFO 3M	Newfoundland-Labrador Shelf
Atlantic cod NAFO 3NO	Newfoundland-Labrador Shelf
Atlantic cod NAFO 3Pn4RS	Newfoundland-Labrador Shelf
Atlantic cod NAFO 3Ps	Newfoundland-Labrador Shelf
Atlantic cod NAFO 4TVn	Scotian Shelf
Atlantic cod NAFO 5Zjm	Northeast U.S. Continental Shelf
Atlantic cod North Sea	North Sea
Atlantic cod Northeast Arctic	Barents Sea & Norwegian Sea
Atlantic cod West of Scotland	Celtic-Biscay Shelf
Atlantic croaker Mid-Atlantic Coast	Southeast U.S. Continental Shelf & Northeast U.S. Continental Shelf
Atlantic herring Northwestern Atlantic Coast	Northeast U.S. Continental Shelf
Atlantic mackerel Gulf of Maine & Cape Hatteras	Northeast U.S. Continental Shelf
Australian salmon New Zealand	New Zealand Shelf
Bigeye tuna Eastern Pacific	North Pacific ocean & South Pacific ocean
Bigeye tuna Western Pacific Ocean	North Pacific ocean & South Pacific ocean
Black Grouper Gulf of Mexico	Gulf of Mexico
Black rockfish Northern Pacific Coast	California Current
Black sea bass Mid-Atlantic Coast	Northeast U.S. Continental Shelf
Blue mackerel East China Sea	East China Sea

Blue marlin Pacific Ocean	North Pacific ocean & South Pacific ocean
Blue Warehou Eastern half of Southeast Australia	East-Central Autralian Shelf & Southwest Australian Shelf
Blue Warehou Western half of Southeast Australia	Southwest Australian Shelf
Bluefin tuna Eastern Atlantic	North Atlantic ocean & South Atlantic ocean
Bluefin tuna Western Atlantic	North Atlantic ocean & South Atlantic ocean
Bluefish Atlantic Coast	Southeast U.S. Continental Shelf & Northeast U.S. Continental Shelf
Cabezon Oregon Coast	California Current
California scorpionfish Southern California	California Current
Canary rockfish Pacific Coast	California Current
Capelin Barents Sea	Barents Sea
Capelin Iceland	Iceland Shelf
Chilean jack mackerel Chilean EEZ and offshore & Humboldt Current	
Chilipepper Southern Pacific Coast	California Current
Chub mackerel Tsushima Strait	East China Sea & Sea of Japan
common European sole Bay of Biscay	Baltic Sea
common European sole Celtic Sea	Celtic-Biscay Shelf
common European sole ICES Kattegat and Skagerrak	North Sea
common European sole ICES VIId	Celtic-Biscay Shelf & North Sea
common European sole Irish Sea	Celtic-Biscay Shelf
common European sole North Sea	North Sea
common European sole Western English Channel	Celtic-Biscay Shelf
common gemfish New Zealand	New Zealand Shelf
common gemfish Southeast Australia	East-Central Australian Shelf & Southwest Australian Shelf
Darkblotched rockfish Pacific Coast	California Current

Deep-water cape hake South Africa	Benguela Current & Agulhas Current
Deepwater flathead Southeast Australia	East-Central Autralian Shelf & Southwest Australian Shelf
Dover sole Gulf of Alaska	Gulf of Alaska
Dover sole Pacific Coast	California Current
Dusky rockfish Gulf of Alaska	Gulf of Alaska
English sole Pacific Coast	California Current
European pilchard ICES VIIIc-IXa	Iberian Coastal
European Plaice ICES IIIa	North Sea
European Plaice ICES VIId	North Sea & Celtic-Biscay Shelf
European Plaice ICES VIIe	Celtic-Biscay Shelf
European Plaice ICES VIIf-g	Celtic-Biscay Shelf
European Plaice Irish Sea	Celtic-Biscay Shelf
European Plaice North Sea	North Sea
Flathead sole Bering Sea and Aleutian Islands	East Bering Sea
Flathead sole Gulf of Alaska	Gulf of Alaska
flounder Inland Sea of Japan	Sea of Japan
Fourspotted megrim ICES VIIIc-IXa	Iberian Coastal
Gag Gulf of Mexico	Gulf of Mexico
Gag Southern Atlantic coast	Southeast U.S. Continental Shelf
Giant stargazer NZ Area STA7	New Zealand Shelf
Golden Redfish Northeast Arctic	Barents Sea & Norwegian Sea
Gopher rockfish Southern Pacific Coast	California Current
Greater amberjack Southern Atlantic coast	Southeast U.S. Continental Shelf
Greenland halibut NAFO 23KLMNO	Newfoundland-Labrador Shelf
Greenland halibut Northeast Arctic	Norwegian Sea & Barents Sea
Haddock Faroe Plateau	Faroe Plateau
Haddock Georges Bank	Northeast U.S. Continental Shelf
Haddock Iceland	Iceland Shelf
Haddock ICES IIIa and North Sea	North Sea
Haddock ICES VIIb-k	Celtic-Biscay Shelf & Iberian Coastal
Haddock Irish Sea	Celtic-Biscay Shelf

Haddock NAFO-4X5Y	Northeast U.S. Continental Shelf & Scotian Shelf
Haddock NAFO-5Y	Northeast U.S. Continental Shelf
Haddock NAFO-5Zejm	Northeast U.S. Continental Shelf
Haddock Northeast Arctic	Norwegian Sea & Barents Sea
Haddock West of Scotland	Celtic-Biscay Shelf
Hake Northeast Atlantic North	North Sea & Celtic-Biscay Shelf
Hake Northeast Atlantic South	Iberian Coastal
Herring Iceland (Summer spawners)	Iceland Shelf
Herring ICES 22-24-IIIa	North Sea & Baltic Sea
Herring ICES 25-32	Baltic Sea
Herring ICES 28	Baltic Sea
Herring ICES 30	Baltic Sea
Herring ICES 31	Baltic Sea
Herring ICES VIa	Celtic-Biscay Shelf
Herring ICES VIa-VIIb-VIIc	Celtic-Biscay Shelf
Herring ICES VIIa-g-h-j	Celtic-Biscay Shelf
Herring NAFO 4R fall spawners	Newfoundland-Labrador Shelf
Herring NAFO 4R spring spawners	Newfoundland-Labrador Shelf
Herring NAFO 4T fall spawners	Scotian Shelf
Herring NAFO 4T spring spawners	Scotian Shelf
Herring North Sea	North Sea
Herring Northern Irish Sea	Celtic-Biscay Shelf
Herring Scotian Shelf and Bay of Fundy	Northeast U.S. Continental Shelf & Scotian Shelf
Hoki Eastern New Zealand	New Zealand Shelf
Hoki Western New Zealand	New Zealand Shelf
Jackass morwong Southeast Australia	East-Central Autralian Shelf & Southwest Australian Shelf
Japanese anchovy Pacific Coast of Japan	Kuroshio Current
Japanese jack mackerel Tsushima Strait	East China Sea & Sea of Japan
Japanese pilchard Tsushima Strait	East China Sea & Sea of Japan

Japanese Spanish mackerel Inland Sea of Japan	Sea of Japan & East Sea
Kelp greenling Oregon Coast	California Current
Lingcod Northern Pacific Coast	California Current
Lingcod Southern Pacific Coast	California Current
Longspine thornyhead Pacific Coast	California Current
Mackerel ICES Northeast Atlantic	Celtic-Biscay Shelf & North Sea & Faroe Plateau
Megrim ICES VIIIc-IXa	Iberian Coastal
Monkfish Southern Georges Bank & Mid-Atlantic	Northeast U.S. Continental Shelf
Mutton snapper Southern Atlantic coast and Gulf of Mexico	Gulf of Mexico & Southeast U.S. Continental Shelf
New Zealand ling Eastern half of Southeast Australia	Southwest Australian Shelf & West-Central Australian Shelf
New Zealand ling New Zealand Area LIN 6b	New Zealand Shelf
New Zealand ling New Zealand Area LIN 72	New Zealand Shelf
New Zealand ling New Zealand Area LIN 7WC - WCSI	New Zealand Shelf
New Zealand ling New Zealand Areas LIN 3 and 4	New Zealand Shelf
New Zealand ling New Zealand Areas LIN 5 and 6	New Zealand Shelf
New Zealand ling Western half of Southeast Australia	Southwest Australian Shelf
New Zealand snapper New Zealand Area 8	New Zealand Shelf
Northern rock sole Eastern Bering Sea and Aleutian Islands	East Bering Sea
Northern rockfish Bering Sea and Aleutian Islands	East Bering Sea
Northern rockfish Gulf of Alaska	Gulf of Alaska
Norway pout North Sea	North Sea
Olive flounder East China Sea	East China Sea
Olive flounder Sea of Japan North	Sea of Japan

Pacific bluefin tuna Pacific Ocean	North Pacific ocean & South Pacific ocean
Pacific chub mackerel Pacific Coast	California Current
Pacific cod Bering Sea and Aleutian Islands	East Bering Sea
Pacific cod Gulf of Alaska	Gulf of Alaska
Pacific hake Pacific Coast	California Current
Pacific halibut North Pacific	Gulf of Alaska
Pacific herring Central Coast	Gulf of Alaska
Pacific herring Prince Rupert District	Gulf of Alaska
Pacific herring Prince William Sound	Gulf of Alaska
Pacific herring Queen Charlotte Islands	Gulf of Alaska
Pacific herring Sitka	Gulf of Alaska
Pacific herring Strait of Georgia	Gulf of Alaska
Pacific herring West Coast of Vancouver Island	Gulf of Alaska
Pacific Ocean perch Eastern Bering Sea and Aleutian Islands	East Bering Sea
Pacific ocean perch Gulf of Alaska	Gulf of Alaska
Pacific sardine Pacific Coast	California Current
Pacific saury Northwest Pacific	Oyashio Current
Patagonian grenadier Southern Argentina	Patagonian Shelf
Patagonian toothfish Macquarie Island	New Zealand Shelf
Patagonian toothfish South Africa Subantarctic Prince Edward Islands	Antarctic
Peruvian anchoveta North-Central Peru	Humboldt Current
Petrale sole Pacific Coast	California Current
Pollock Faroe Plateau	Faroe Plateau
Pollock ICES IIIa, VI and North Sea	North Sea
Pollock NAFO-4X5YZ	Northeast U.S. Continental Shelf & Scotian Shelf
Pollock Northeast Arctic	Barents Sea & Norwegian Sea
Pollock or saithe Iceland Grounds	Iceland Shelf
Red grouper Gulf of Mexico	Gulf of Mexico

Red porgy Southern Atlantic coast	Southeast U.S. Continental Shelf
Red seabream Inland Sea of Japan	Sea of Japan
Red seabream Pacific Ocean	East China Sea
Red snapper Eastern Gulf of Mexico	Gulf of Mexico
Red snapper Southern Atlantic coast	Gulf of Mexico & Southeast U.S. Continental Shelf
Red snapper Western Gulf of Mexico	Gulf of Mexico
Redfish species NAFO 3M	Newfoundland-Labrador Shelf
Rex sole Gulf of Alaska	Gulf of Alaska
Rock sole Hecate Strait	Gulf of Alaska
Rougheye rockfish Bering Sea and Aleutian Islands	East Bering Sea
Rougheye rockfish Gulf of Alaska	Gulf of Alaska
Sablefish Eastern Bering Sea & Aleutian Islands & Gulf of Alaska	East Bering Sea & Gulf of Alaska
Sablefish Pacific Coast	California Current
Sandeel North Sea Area 1	North Sea
Sandeel North Sea Area 2	North Sea
Sandeel North Sea Area 3	North Sea
Sardine South Africa	Benguela Current & Agulhas Current
Scami Bay of Plenty	New Zealand Shelf
Scampi Wairapa & Hawke Bay	New Zealand Shelf
School whiting Southeast Australia	Southwest Australian Shelf & West-Central Australian Shelf
Scup Atlantic Coast	North east U.S. Continental Shelf
Sea bream Sea of Japan	Sea of Japan
Shallow-water cape hake South Africa	Benguela Current & Agulhas Current
Shortbelly rockfish Pacific Coast	California Current
Shortspine thornyhead Pacific Coast	California Current
Silverfish Southeast Australia	Southwest Australian Shelf & East-Central Australian Shelf
Snapper Northern Spencer Gulf	Southwest Australian Shelf
Snapper Southern Gulf St. Vincent	Southwest Australian Shelf

Snapper Southern Spencer Gulf	Southwest Australian Shelf
Snowy grouper Southern Atlantic coast	Southeast U.S. Continental Shelf & Caribbean Sea & North Brazil Shelf & East Brazil Shelf
Southern blue whiting Campbell Island Rise	New Zealand Shelf
Southern blue whiting Southern Argentina	Patagonian Shelf
Southern bluefin tuna Southern Oceans	South Atlantic ocean & South Pacific ocean
Southern hake Chatham Rise	New Zealand Shelf
Southern hake Sub-Antarctic	New Zealand Shelf
Southern spiny lobster South Africa South coast	Benguela Current & Agulhas Current
Spanish mackerel Southern Atlantic Coast	Southeast U.S. Continental Shelf
Spiny dogfish Atlantic Coast	Northeast U.S. Continental Shelf & Scotian Shelf & Newfoundland-Labrador
Splitnose Rockfish Pacific Coast	California Current
Sprat ICES Baltic Areas 22-32	Baltic Sea
Starry flounder Northern Pacific Coast	California Current
Starry flounder Southern Pacific Coast	California Current
Striped bass Gulf of Maine & Cape Hatteras	Southeast U.S. Continental Shelf & Northeast U.S.
Striped marlin North Pacific	North Pacific ocean
Striped marlin Northeast Pacific	North Pacific ocean
Striped marlin Western and Central North Pacific	North Pacific ocean & South Pacific ocean
Summer flounder Mid-Atlantic Coast	Southeast U.S. Continental Shelf & Northeast U.S.
Swordfish Eastern Pacific North Pacific ocean & South Pacific ocean	
Swordfish Indian Ocean	Indian ocean
Swordfish North Pacific	North Pacific ocean
Tarakihi New Zealand	New Zealand Shelf

Tilefish Southern Atlantic coast	Northeast U.S. Continental Shelf & Southeast U.S. Continental Shelf & Gulf of Mexico
Trevally New Zealand Areas TRE 7	New Zealand Shelf
Walleye pollock Aleutian Islands	East Bering Sea
Walleye pollock Eastern Bering Sea	East Bering Sea
Walleye pollock Gulf of Alaska	Gulf of Alaska
White hake Georges Bank & Gulf of Maine	Northeast U.S. Continental Shelf
White marlin Atlantic	North Atlantic ocean & South Atlantic ocean
Whiting ICES IIIa, VIId and North Sea	North Sea
Whiting ICES VIa	Celtic-Biscay Shelf
Whiting ICES VIIe-k	Celtic-Biscay Shelf
Whiting Northeast Atlantic	Celtic-Biscay Shelf & North Sea & Norwegian Sea & Barents Sea & Faroe Plateau & Iceland Shelf
Widow rockfish Pacific Coast	California Current
Winter Flounder NAFO-5Z	Northeast U.S. Continental Shelf
Winter Flounder Southern New England-Mid Atlantic	Northeast U.S. Continental Shelf
Witch Flounder NAFO-5Y	Gulf of Alaska
Yellowfin sole Bering Sea and Aleutian Islands	East Bering Sea
Yellowfin tuna Eastern Pacific	North Pacific ocean & South Pacific ocean
Yellowfin tuna Indian Ocean	Indian ocean
Yellowtail flounder Cape Cod & Gulf of Maine	Northeast U.S. Continental Shelf
Yellowtail flounder Georges Bank	Northeast U.S. Continental Shelf
Yellowtail Flounder Southern New England-Mid Atlantic	Northeast U.S. Continental Shelf
Yellowtail rockfish Northern Pacific Coast	California Current
Yellowtail snapper Southern Atlantic Coast	Gulf of Mexico & Southeast U.S. Continental Shelf

Appendix B

Methods for Chapter 3

Rebuilding global fisheries under nonstationary productivity

B.1 Data

To analyze total productivity, data were extracted from the RAM Legacy Stock Assessment Database [25]. This is a global, quality controlled database, available publically at http://ramlegacy.marinebiodiversity.ca/. Stock assessments provide estimates of both total stock biomass (kg) and catch (kg). We analyzed 211 of the 420 time series available in the database. This subset was chosen according to: 1) Visually inspection to determine if the assessment data do not represent purely deterministic model output; and 2) The biomass time series must be estimated directly, as opposed to those based on indirect proxies. A list of species used in the analysis, along with their designated LME can be found in Table B.1.

B.2 Population dynamics

We model the biomass dynamics using the discrete logistic model minus catch which gives the canonical Graham-Schaefer model

$$B_{t+1} = B_t + rB_t\left(1 - \frac{K}{B_t}\right) - C_t, \tag{B.1}$$

where r is the intrinsic productivity and K is the carrying capacity.

The observed surplus production for this model is defined by $B_{t+1} - B_t + C_t$ which represents the total change in biomass. At equilibrium $B_{t+1} - B_t = 0$, the catch is equal to surplus production and therefore maximizing catch is equal to maximizing $rB_t(1 - K/B_t)$ which provides the maximum sustainable yield of the resource. This results in the biomass that produces MSY

$$\mathrm{B_{MSY}} = \frac{1}{2}K.$$

Substituting this quantity into the logistic model yields MSY

$$\mathrm{MSY} = rB_{MSY}\left(1 - \frac{B_{MSY}}{K}\right) = r\frac{K}{4}.$$

Rebuilding times were calculated as the time (in years) to exceed $\mathrm{B_{MSY}}$ when a stock is depleted below. Our expression for rebuilding time depends on the solution to the continuous form of B.1. To derive rebuilding time, we first solve the initial value problem for the continuous Graham-Schaefer with the initial condition $B = B_0$. Setting the solution equal to $\mathrm{B_{MSY}}$ we arrive at the expression for the number of years to rebuilding as a function of the initial condition $B_0/\mathrm{B_{MSY}}$, the intrinsic productivity, and the level of fishing mortality

$$t = \ln\left(\frac{\frac{2\mathrm{B_{MSY}}\left(1 - \frac{F}{r}\right)}{B_0} - 1}{1 - \frac{2F}{r}}\right)\frac{1}{r - F}$$

B.3 State space model parameterization

Using estimates of annual biomass B and catch C, and fixing K at the maximum observed catch plus biomass to focus on productivity, we solve for the annually observed intrinsic productivity and model the observed value as a true biological rate plus annual noise

$$r_t^{obs} = \frac{K(B_t - B_{t+1} - C_t)}{B_t(B_t - K)} = r_t^{true} + e_t^{obs}.$$

We assume that the biological rate evolves as a random walk with an underlying trend, expressed as a stochastic difference equation

$$\mathbf{r_t} = \mathbf{D r_{t-1}} + \mathbf{e_t^r} = \begin{bmatrix} r_t \\ \Delta r \end{bmatrix} = \begin{bmatrix} 1 & 1 \\ 0 & 1 \end{bmatrix} \begin{bmatrix} r_{t-1} \\ \Delta r \end{bmatrix} + \begin{bmatrix} e_t^r \\ 0 \end{bmatrix},$$

The time-varying biological rates are modelled as a Gaussian process to be estimated using the Kalman filter and smoother [23, 24]. For the Bayesian implementation, we utilize the conjugate Gaussian-inverse-gamma parameterization [23] for the probability distributions

$$e_t^{obs} \mid \phi_{\sigma^2_{obs}} \sim Gaussian(0, \sigma^2_{obs} = \phi^{-1}_{\sigma^2_{obs}}),$$

$$\mathbf{e_t^r} \mid \phi_r \sim Gaussian(\mathbf{0}, \mathbf{\Sigma} = \text{diag}(\sigma_r^2 = \phi_r^{-1}, \sigma^2_{\Delta r} = 0_{\Delta r})),$$

$$\phi_{\sigma^2_{obs}} \sim Gamma(\alpha_{\sigma^2_{obs}}, \beta_{\sigma^2_{obs}}),$$

$$\phi_r \sim Gamma(\alpha_r, \beta_r),$$

where the notion $\sim Gaussian(x, y)$ reads 'is Gaussian distributed with mean parameter x and variance parameter y', $\sim Gamma(x, y)$ reads 'is gamma distributed with shape

parameter x and scale parameter y'. The bold face type represents a multivariate vector or matrix based on its context. The model parameterizes r_t as a random walk with variance ϕ_r^{-1} and constant slope Δr. Hence $\mathbf{\Sigma} = \text{diag}(\phi_r^{-1}, 0_{\Delta r})$ meaning Δr has no variance with respect to time and is assumed fixed. For priors, I assigned $\alpha_{\sigma^2_{obs}}, \beta_{\sigma^2_{obs}}, \alpha_r, \beta_r$ on a stock by stock basis to satisfy the following informative conditions: 1) Zero probability at zero observation and process variance; and 2) broad probability between zero and a value that represented $\frac{1}{2}$ standard deviation of the raw time series. That is, I chose prior densities such that the observation error standard deviation σ_{obs} was primarily constrained between $(0, \frac{1}{2}\, sd(B))$ and fell away quickly thereafter (i.e. maximum possible observation error equal to half the standard deviation of biomass). Priors for σ_r were similarly constrained between $(0, \frac{1}{2}\, sd(r_{obs})$. These represent mildly informative 'empirical' priors that bound variances within reasonable values but give no relative weight to observation or process error.

B.4 State space model estimation

The conjugacy of the Gaussian-inverse-gamma parameterization results in gamma distributed posterior conditional distributions

$$\phi_{\sigma^2_{obs}} \mid r_t^{obs} \sim Gamma\left(\{\alpha_{\sigma^2_{obs}} + \frac{T}{2}\},\ \{\beta_{\sigma^2_{obs}} + \frac{1}{2}\sum_{t=1}^{T}(r_t^{obs} - \mathbf{Hr_t})^2\}\right),$$

$$\phi_r \mid r_t^{obs} \sim Gamma\left(\{\alpha_r + \frac{T}{2}\},\ \{\beta_r + \frac{1}{2}\sum_{t=1}^{T}(\mathbf{r_t} - \mathbf{Dr_{t-1}})^2\}\right),$$

which can be sampled directly using standard Gibbs MCMC sampling in order to build the joint and marginal posterior distributions. All computations were performed in **R**.

B.5 Recovery time

With the marginal posterior samples of r_t, the posterior predictive distribution for recovery time t is found by propagating the samples through the recovery time equation.

B.6 Basic R code

```
################################################################################
################################################################################
## This code performs Bayesian inference on linear Gaussian state space model - ##
## The model is defined as a random walk + slope ------------------------------ ##
## The code specifies priors and storage space, then performs Gibbs sampling -- ##
## \\ by successively conditioning on each unknown parameters and sampling ---- ##
## \\ the conditional distribution -------------------------------------------- ##
## Note that the code below makes use of a 'Filter' function which runs ------- ##
## \\ the Kalman filter, conditional on R and Q ------------------------------- ##
## The code to run the Kalman filter is given in Appendix A and --------------- ##
## \\ with suitable re-specification of matrices D and H ---------------------- ##
################################################################################
################################################################################

n.data <- length(data)

MC     <- 100
keep   <- 1:MC
n.keep <- length(keep)

# Priors
sigma_obs_shape <- 2
sigma_obs_rate  <- 0.01
sigma_state_shape <- 2
sigma_state_rate <- 4

# Storage
state_post <- array(NA, dim=c(n.keep, n.data + 1, 2))
sigma_obs_post <- rep(NA, n.keep)
sigma_state_post  <- rep ( NA, n.keep )

# Gibbs Sampler
for ( i in 1:MC )
{
        # Sample states conditional on R and Q
        theta <- Filter(data, R, Q)
        theta.pred <- theta[-n.data+1,]%*%t(D)
        theta.res <- theta[-1,] - theta.pred

        # Sample R conditional on states and Q
        fit <- theta[-1,] %*% t(H)
        rss <- sum ((data-fit)^2)
        R_prime <- rgamma(1, shape = sigma_obs_shape + n.data/2,
                rate = sigma_obs_rate + rss/2)
        R <- 1/R_prime
```

```
        # Sample Q conditional on states and R
        rss <- sum(theta.res[,2]^2)
        Q_prime <- rgamma(1, shape = sigma_state_shape + n.data/2,
                rate = sigma_state_rate + rss/2)
        Q <- 1/Q_prime

        # Store
        state_post[j,,] <- theta
        sigma_obs_post[j] <- R
        sigma_state_post[j] <- Q

}
```

,

Table B.1. Stocks used in the analysis of total productivity

Common Stock ID [25]	**Large Marine Ecosystem**
Albacore tuna South Pacific Ocean	South Pacific ocean
American Plaice NAFO-3LNO	Newfoundland-Labrador Shelf
American Plaice NAFO-3M	Newfoundland-Labrador Shelf
American Plaice NAFO-5YZ	Northeast U.S. Continental Shelf & Scotian Shelf
Anchovy kilka Caspian Sea	Black Sea
Anchovy South Africa	Benguela Current & Agulhas Current
Argentine hake Northern Argentina	Patagonian Shelf & South Brazil Shelf
Argentine hake Southern Argentina	Patagonian Shelf
Atka mackerel Bering Sea and Aleutian Islands	East Bering Sea
Atlantic cod Baltic Areas 22 and 24	Baltic Sea
Atlantic cod Baltic Areas 25-32	Baltic Sea
Atlantic cod coastal Norway	Barents Sea & Norwegian Sea
Atlantic cod Faroe Plateau	Faroe Plateau
Atlantic cod Georges Bank	Northeast U.S. Continental Shelf
Atlantic cod Gulf of Maine	Northeast U.S. Continental Shelf
Atlantic cod Iceland	Iceland Shelf
Atlantic cod Irish Sea	Celtic-Biscay Shelf
Atlantic cod Kattegat	North Sea
Atlantic cod NAFO 2J3KL inshore	Newfoundland-Labrador Shelf
Atlantic cod NAFO 3NO	Newfoundland-Labrador Shelf
Atlantic cod NAFO 3Pn4RS	Newfoundland-Labrador Shelf
Atlantic cod NAFO 3Ps	Newfoundland-Labrador Shelf
Atlantic cod NAFO 4TVn	Scotian Shelf
Atlantic cod NAFO 5Zjm	Northeast U.S. Continental Shelf
Atlantic cod North Sea	North Sea
Atlantic cod Northeast Arctic	Barents Sea & Norwegian Sea
Atlantic cod West of Scotland	Celtic-Biscay Shelf

Atlantic menhaden Atlantic	Southeast U.S. Continental Shelf & Northeast U.S. Continental Shelf
Bigeye tuna Western Pacific Ocean	Western Pacific ocean
Black sea bass Mid-Atlantic Coast	Northeast U.S. Continental Shelf
Bluefin tuna Eastern Atlantic	North Atlantic ocean & South Atlantic ocean
Bluefish Atlantic Coast	Southeast U.S. Continental Shelf & Northeast U.S. Continental Shelf
Capelin Barents Sea	Barents Sea
Capelin Iceland	Iceland Shelf
common European sole Bay of Biscay	Baltic Sea
common European sole Celtic Sea	Celtic-Biscay Shelf
common European sole ICES Kattegat and Skagerrak	North Sea
common European sole ICES VIId	Celtic-Biscay Shelf
common European sole ICES VIId	North Sea
common European sole Irish Sea	Celtic-Biscay Shelf
common European sole Western English Channel	Celtic-Biscay Shelf
common gemfish New Zealand	New Zealand Shelf
common gemfish Southeast Australia	East Central Australian Shelf & Southeast Australian Shelf
English sole Hecate Strait	Gulf of Alaska
European Plaice ICES VIIe	Celtic-Biscay Shelf
European Plaice ICES VIIf-g	Celtic-Biscay Shelf
European Plaice Irish Sea	Celtic-Biscay Shelf
Flathead sole Bering Sea and Aleutian Islands	East Bering Sea
Fourspotted megrim ICES VIIIc-IXa	Iberian Coastal
Gag Gulf of Mexico	Gulf of Mexico
Golden Redfish Northeast Arctic	Barents Sea & Norwegian Sea
Gopher rockfish Southern Pacific Coast	California Current
Greenland halibut NAFO 23KLMNO	Newfoundland-Labrador Shelf

Greenland halibut Northeast Arctic	Norwegian Sea & Barents Sea
Gulf menhaden Gulf of Mexico	Gulf of Mexico
Haddock Faroe Plateau	Faroe Plateau
Haddock Georges Bank	Northeast U.S. Continental Shelf
Haddock Iceland	Iceland Shelf
Haddock ICES IIIa and North Sea	North Sea
Haddock ICES VIIb-k	Celtic-Biscay Shelf
Haddock ICES VIIb-k	Iberian Coastal
Haddock Irish Sea	Celtic-Biscay Shelf
Haddock NAFO-4X5Y	Northeast U.S. Continental Shelf & Scotian Shelf
Haddock NAFO-5Y	Northeast U.S. Continental Shelf
Haddock NAFO-5Zejm	Northeast U.S. Continental Shelf
Haddock Northeast Arctic	Norwegian Sea & Barents Sea
Haddock Rockall Bank	Faroe Plateau
Haddock West of Scotland	Celtic-Biscay Shelf
Hake Northeast Atlantic North	North Sea
Hake Northeast Atlantic North	Celtic-Biscay Shelf
Herring Iceland (Summer spawners)	Iceland Shelf
Herring ICES 22-24-IIIa	North Sea
Herring ICES 22-24-IIIa	Baltic Sea
Herring ICES 25-32	Baltic Sea
Herring ICES 28	Baltic Sea
Herring ICES 30	Baltic Sea
Herring ICES 31	Baltic Sea
Herring ICES VIa	Celtic-Biscay Shelf
Herring ICES VIa-VIIb-VIIc	Celtic-Biscay Shelf
Herring NAFO 4R spring spawners	Newfoundland-Labrador Shelf
Herring NAFO 4T fall spawners	Scotian Shelf
Herring NAFO 4T spring spawners	Scotian Shelf
Herring North Sea	North Sea
Herring Northern Irish Sea	Celtic-Biscay Shelf
Hoki Eastern New Zealand	New Zealand Shelf

Hoki Western New Zealand	New Zealand Shelf
King mackerel Gulf of Mexico	Gulf of Mexico
King mackerel Southern Atlantic Coast	Southeast U.S. Continental Shelf
Longspine thornyhead Pacific Coast	California Current
Mackerel ICES Northeast Atlantic	Celtic-Biscay Shelf & North Sea & Faroe Plateau
Megrim ICES VIIIc-IXa	Iberian Coastal
Monkfish Gulf of Maine & Northern Georges Bank	Northeast U.S. Continental Shelf
New Zealand ling New Zealand Area LIN 6b	New Zealand Shelf
New Zealand ling New Zealand Area LIN 72	New Zealand Shelf
New Zealand ling New Zealand Area LIN 7WC - WCSI	New Zealand Shelf
New Zealand ling New Zealand Areas LIN 3 and 4	New Zealand Shelf
New Zealand ling New Zealand Areas LIN 5 and 6	New Zealand Shelf
Northern rockfish Bering Sea and Aleutian Islands	East Bering Sea
Norway pout North Sea	North Sea
Pacific cod Bering Sea and Aleutian Islands	East Bering Sea
Pacific cod Gulf of Alaska	Gulf of Alaska
Pacific cod Hecate Strait	Gulf of Alaska
Pacific cod West Coast of Vancouver Island	Gulf of Alaska
Pacific hake Pacific Coast	California Current
Pacific halibut North Pacific	Gulf of Alaska
Pacific herring Central Coast	Gulf of Alaska
Pacific herring Prince Rupert District	Gulf of Alaska
Pacific herring Prince William Sound	Gulf of Alaska
Pacific herring Queen Charlotte Islands	Gulf of Alaska
Pacific herring Sitka	Gulf of Alaska
Pacific herring Straight of Georgia	Gulf of Alaska

Pacific herring West Coast of Vancouver Island	Gulf of Alaska
Pacific Ocean perch Eastern Bering Sea and Aleutian Islands	East Bering Sea
Pacific sardine Pacific Coast	California Current
Patagonian grenadier Southern Argentina	Patagonian Shelf
Pollock Faroe Plateau	Faroe Plateau
Pollock ICES IIIa, VI and North Sea	North Sea
Pollock NAFO-4X5YZ	Northeast U.S. Continental Shelf & Scotian Shelf
Pollock Northeast Arctic	Barents Sea & Norwegian Sea
Red grouper Gulf of Mexico	Gulf of Mexico
Red porgy Southern Atlantic coast	Southeast U.S. Continental Shelf
Redfish species NAFO 3M	Newfoundland-Labrador Shelf
Rex sole Gulf of Alaska	Gulf of Alaska
Rock sole Hecate Strait	Gulf of Alaska
Rougheye rockfish Gulf of Alaska	Gulf of Alaska
Sablefish	Eastern Bering Sea & Aleutian Islands & Gulf of Alaska & East Bering Sea & Gulf of Alaska
Silverfish Southeast Australia	Southeast Australian Shelf & East Central Australian Shelf
Snowy grouper Southern Atlantic coast	Southeast U.S. Continental Shelf & Caribbean Sea & North Brazil Shelf & East Brazil Shelf
Southern blue whiting Campbell Island Rise	New Zealand Shelf
Southern hake Chatham Rise	New Zealand Shelf
Southern hake Sub-Antarctic	New Zealand Shelf
Southern spiny lobster South Africa South coast	Benguela Current & Agulhas Current
Spanish mackerel Southern Atlantic Coast	Southeast U.S. Continental Shelf
Spiny dogfish Atlantic Coast	Northeast U.S. Continental Shelf & Scotian Shelf & Newfoundland-Labrador Shelf

Sprat ICES Baltic Areas 22-32	Baltic Sea
Summer flounder Mid-Atlantic Coast	Southeast U.S. Continental Shelf & Northeast U.S. Continental Shelf
Tasmanian giant crab Tasmania	Southeast Australian Shelf
Tilefish Southern Atlantic coast	Northeast U.S. Continental Shelf & Southeast U.S. Continental Shelf & Gulf of Mexico
Trevally New Zealand Areas TRE 7	New Zealand Shelf
Walleye pollock Eastern Bering Sea	East Bering Sea
White hake Georges Bank & Gulf of Maine	Northeast U.S. Continental Shelf
Whiting ICES IIIa, VIId and North Sea	North Sea
Whiting ICES VIIe-k	Celtic-Biscay Shelf
Whiting Northeast Atlantic Celtic-Biscay Shelf & North Sea & Norwegian Sea & Barents Sea & Faroe Plateau	Iceland Shelf
Winter Flounder NAFO-5Z	Northeast U.S. Continental Shelf
Winter Flounder Southern New England-Mid Atlantic	Northeast U.S. Continental Shelf
Yellowtail flounder Cape Cod & Gulf of Maine	Northeast U.S. Continental Shelf
Yellowtail flounder Georges Bank	Northeast U.S. Continental Shelf
Yellowtail Flounder Southern New England-Mid Atlantic	Northeast U.S. Continental Shelf
Yellowtail rockfish Northern Pacific Coast	California Current

Bibliography

1. FAO, *The Status of World Fisheries and Aquaculture*. United Nations Food And Agriculture Organisation, 2012.

2. S. C. Walpole, D. Prieto-Merino, P. Edwards, J. Cleland, G. Stevens, and I. Roberts, "The weight of nations: an estimation of adult human biomass.," *BMC public health*, vol. 12, p. 439, Jan. 2012.

3. C. Mora, A. G. Frazier, R. J. Longman, R. S. Dacks, M. M. Walton, E. J. Tong, J. J. Sanchez, L. R. Kaiser, Y. O. Stender, J. M. Anderson, C. M. Ambrosino, I. Fernandez-Silva, L. M. Giuseffi, and T. W. Giambelluca, "The projected timing of climate departure from recent variability.," *Nature*, vol. 502, pp. 183–7, Oct. 2013.

4. P. L. Munday, D. L. Dixson, M. I. Mccormick, M. Meekan, M. C. O. Ferrari, and D. P. Chivers, "Replenishment of fish populations is threatened by ocean acidification," *Proceedings of the National Academy of Sciences*, vol. 107, no. 29, pp. 12930–12934, 2010.

5. C. Mora, C.-L. Wei, A. Rollo, T. Amaro, A. R. Baco, D. Billett, L. Bopp, Q. Chen, M. Collier, R. Danovaro, A. J. Gooday, B. M. Grupe, P. R. Halloran, J. Ingels, D. O. B. Jones, L. a. Levin, H. Nakano, K. Norling, E. Ramirez-Llodra, M. Rex, H. a. Ruhl, C. R. Smith, A. K. Sweetman, A. R. Thurber, J. F. Tjiputra, P. Usseglio, L. Watling, T. Wu, and M. Yasuhara, "Biotic and human vulnerability to projected changes in ocean biogeochemistry over the 21st century.," *PLoS biology*, vol. 11, p. e1001682, Oct. 2013.

6. R. F. Keeling, A. Körtzinger, and N. Gruber, "Ocean Deoxygenation in a Warming World," *Annual Review of Marine Science*, vol. 2, pp. 199–229, Jan. 2010.

7. N. Gruber, "Warming up, turning sour, losing breath: ocean biogeochemistry under global change.," *Philosophical transactions of the Royal Society A*, vol. 369, pp. 1980–96, May 2011.

8. R. J. Nicholls and A. Cazenave, "Sea-level rise and its impact on coastal zones.," *Science*, vol. 328, pp. 1517–20, June 2010.

9. P. M. Cury, Y.-J. Shin, B. Planque, J. M. Durant, J.-M. Fromentin, S. Kramer-Schadt, N. C. Stenseth, M. Travers, and V. Grimm, "Ecosystem oceanography for global change in fisheries," *Trends in ecology and evolution*, vol. 23, pp. 338–346, June 2008.

10. W. W. Cheung, V. W. Lam, J. L. Sarmiento, K. Kearney, R. Watson, and D. Pauly, "Projecting global marine biodiversity impacts under climate change scenarios," *Fish and Fisheries*, vol. 10, pp. 235–251, Sept. 2009.

11. E. H. Allison, A. L. Perry, M.-C. Badjeck, W. Neil Adger, K. Brown, D. Conway, A. S. Halls, G. M. Pilling, J. D. Reynolds, N. L. Andrew, and N. K. Dulvy, "Vulnerability of national economies to the impacts of climate change on fisheries," *Fish and Fisheries*, vol. 10, pp. 173–196, June 2009.

12. E. S. Poloczanska, C. J. Brown, W. J. Sydeman, W. Kiessling, D. S. Schoeman, P. J. Moore, K. Brander, J. F. Bruno, L. B. Buckley, M. T. Burrows, C. M. Duarte, B. S. Halpern, J. Holding, C. V. Kappel, M. I. OConnor, J. M. Pandolfi, C. Parmesan, F. Schwing, S. A. Thompson, and A. J. Richardson, "Global imprint of climate change on marine life," *Nature Climate Change*, vol. 3, pp. 919–925, Aug. 2013.

13. S. R. Carpenter, J. J. Cole, M. L. Pace, R. Batt, W. A. Brock, T. Cline, J. Coloso, J. R. Hodgson, J. F. Kitchell, D. a. Seekell, L. Smith, and B. Weidel, "Early warnings of regime shifts: a whole-ecosystem experiment.," *Science*, vol. 332, pp. 1079–82, May 2011.

14. M. Scheffer, J. Bascompte, W. A. Brock, V. Brovkin, S. R. Carpenter, V. Dakos, H. Held, E. H. van Nes, M. Rietkerk, and G. Sugihara, "Early-warning signals for critical transitions.," *Nature*, vol. 461, pp. 53–9, Sept. 2009.

15. N. Mantua, S. R. Hare, Y. Zhang, J. M. Wallace, and R. C. Francis, "A Pacific interdecadal climate oscillation with impacts on salmon production," *Bulletin of the American Meterological Society*, vol. 78, no. 6, pp. 1069–1079, 1997.

16. S. R. Carpenter, W. A. Brock, J. J. Cole, J. F. Kitchell, and M. L. Pace, "Leading indicators of trophic cascades.," *Ecology letters*, vol. 11, pp. 128–38, Feb. 2008.

17. A. Hastings and D. B. Wysham, "Regime shifts in ecological systems can occur with no warning.," *Ecology letters*, vol. 13, pp. 464–72, Apr. 2010.

18. M. Scheffer, S. R. Carpenter, T. M. Lenton, J. Bascompte, W. Brock, V. Dakos, J. van de Koppel, I. A. van de Leemput, S. A. Levin, E. H. van Nes, M. Pascual, and J. Vandermeer, "Anticipating critical transitions.," *Science*, vol. 338, pp. 344–8, Oct. 2012.

19. R. Wang, J. A. Dearing, P. G. Langdon, E. Zhang, X. Yang, V. Dakos, and M. Scheffer, "Flickering gives early warning signals of a critical transition to a eutrophic lake state.," *Nature*, vol. 492, pp. 419–22, Dec. 2012.

20. C. J. Walters, "Nonstationarity of production realtionships in exploited populations," *Canadian Journal of Fisheries and Aquatic Sciences*, vol. 44, pp. 156–165, 1987.

21. Z. Chen, "Bayesian filtering: From Kalman filters to particle filters, and beyond," *Statistics*, vol. 1, pp. 1–69, 2003.

22. R. K. Mehra, "Approaches to adaptive filtering," *IEEE Transaction on Automatic Control*, vol. 17, pp. 693–698, 1972.

23. G. Petris, S. Petrone, and P. Campagnoli, *Dynamic linear model with R*. New York: Springer, 2009.

24. J. Durbin and S. J. Koopman, *Time Series Analysis by State Space Methods*. Oxford: Oxford University Press, 2008.

25. D. Ricard, C. Minto, O. P. Jensen, and J. K. Baum, "Examining the knowledge base and status of commercially exploited marine species with the RAM Legacy Stock Assessment Database," *Fish and Fisheries*, vol. 13, pp. 380–398, Dec. 2012.

26. R. Hilborn and C. J. Walters, *Quantitative fisheries stock assessment: Choice, dynamics and uncertainty*, vol. 2. New York, NY: Chapman and Hall/CRC, June 1992.

27. W. W. L. Cheung, V. W. Y. Lam, J. L. Sarmiento, K. Kearney, R. Watson, D. Zeller, and D. Pauly, "Large-scale redistribution of maximum fisheries catch potential in the global ocean under climate change," *Global Change Biology*, vol. 16, pp. 24–35, Jan. 2010.

28. W. W. L. Cheung, J. L. Sarmiento, J. Dunne, T. L. Frölicher, V. W. Y. Lam, M. L. Deng Palomares, R. Watson, and D. Pauly, "Shrinking of fishes exacerbates impacts of global ocean changes on marine ecosystems," *Nature Climate Change*, vol. 3, pp. 254–258, Sept. 2012.

29. D. G. Boyce, M. Dowd, M. R. Lewis, and B. Worm, "Estimating global chlorophyll changes over the past century," *Progress in Oceanography*, vol. 122, pp. 163–173, 2014.

30. W. W. L. Cheung, R. Watson, and D. Pauly, "Signature of ocean warming in global fisheries catch.," *Nature*, vol. 497, pp. 365–8, May 2013.

31. M. L. Pinsky, B. Worm, M. J. Fogarty, J. L. Sarmiento, and S. A. Levin, "Marine taxa track local climate velocities.," *Science*, vol. 341, pp. 1239–42, Sept. 2013.

32. I. M. Belkin, "Rapid warming of large marine ecosystems," *Progress in Oceanography*, vol. 81, pp. 207–213, Apr. 2009.

33. D. G. Boyce, M. Lewis, and B. Worm, "Integrating global chlorophyll data from 1890 to 2010," *Limnology and Oceanography: Methods*, vol. 10, pp. 840–852, 2012.

34. D. O. Conover and S. B. Munch, "Sustaining fisheries yields over evolutionary time scales," *Science*, vol. 297, pp. 94–96, July 2002.

35. E. M. Olsen, M. Heino, G. R. Lilly, M. J. Morgan, J. Brattey, B. Ernade, and U. Dieckmann, "Maturation trends indicative of rapid evolution preceded the collapse of northern cod," *Nature*, vol. 428, pp. 932–935, 2004.

36. R. M. Peterman, B. J. Pyper, and B. W. Macgregor, "Use of the Kalman filter to reconstruct historical trends in productivity of Bristol Bay sockeye salmon," vol. 824, pp. 809–824, 2003.

37. C. Minto, J. M. Flemming, G. L. Britten, and B. Worm, "Productivity dynamics of Atlantic cod," *Canadian Journal of Fisheries and Aquatic Sciences*, vol. 216, pp. 203–216, 2014.

38. A. O. Shelton, S. B. Munch, D. Keith, and M. Mangel, "Maternal age, fecundity, egg quality, and recruitment: linking stock structure to recruitment using an age-structured Ricker model," *Canadian Journal of Fisheries and Aquatic Sciences*, vol. 69, no. 10, pp. 1631–1641, 2012.

39. T. Platt, C. Fuentes-Yaco, and K. T. Frank, "Spring algal bloom and larval fish survival," *Nature*, vol. 423, pp. 398–399, 2003.

40. B. Worm, R. Hilborn, J. K. Baum, T. A. Branch, J. S. Collie, C. Costello, M. J. Fogarty, E. a. Fulton, J. A. Hutchings, S. Jennings, O. P. Jensen, H. K. Lotze, P. M. Mace, T. R. McClanahan, C. Minto, S. R. Palumbi, A. M. Parma, D. Ricard, A. a. Rosenberg, R. Watson, D. Zeller, and E. al., "Rebuilding global fisheries," *Science*, vol. 325, pp. 578–585, July 2009.

41. A. McCrea-Strub, K. Kleisner, U. R. Sumaila, W. Swartz, R. Watson, D. Zeller, and D. Pauly, "Potential impact of the deepwater horizon oil spill on commercial fisheries in the Gulf of Mexico," *Fisheries*, vol. 36, no. 7, pp. 332–336, 2011.

42. C. Costello, D. Ovando, R. Hilborn, S. D. Gaines, O. Deschenes, and S. E. Lester, "Status and solutions for the world's unassessed fisheries.," *Science*, vol. 338, pp. 517–20, Oct. 2012.

43. C. N. K. Anderson, C.-h. Hsieh, S. A. Sandin, R. Hewitt, A. Hollowed, J. Beddington, R. M. May, and G. Sugihara, "Why fishing magnifies fluctuations in fish abundance.," *Nature*, vol. 452, pp. 835–9, Apr. 2008.

44. A. O. Shelton and M. Mangel, "Fluctuations of fish populations and the magnifying effects of fishing," *Proceedings of the National Academy of Sciences*, vol. 108, pp. 7075–7080, Apr. 2011.

45. M. P. Hassell, "Density-dependence in single-species populations," *Journal of Animal Ecology*, vol. 44, no. 1, pp. 283–295, 1975.

46. D. Pauly, V. Christensen, J. Dalsgaard, R. Froese, and F. Torres Jr., "Fishing down marine food webs," *Science*, vol. 279, no. 5352, pp. 860–863, 1998.

47. B. Worm, E. B. Barbier, N. Beaumont, J. E. Duffy, C. Folke, B. S. Halpern, J. B. C. Jackson, H. K. Lotze, F. Micheli, S. R. Palumbi, E. Sala, K. a. Selkoe, J. J. Stachowicz, and R. Watson, "Impacts of biodiversity loss on ocean ecosystem services.," *Science*, vol. 314, pp. 787–90, Nov. 2006.

48. P. Neubauer, O. P. Jensen, J. A. Hutchings, and J. K. Baum, "Resilience and recovery of overexploited marine populations," *Science*, vol. 340, pp. 347–349, Apr. 2013.

49. C. Safina, A. A. Rosenberg, R. A. Myers, T. J. Quinn II, and J. S. Collie, "U.S. Ocean fish recovery: Staying the course," *Science*, vol. 27, no. 29, p. 64, 2005.

50. D. Cressey, "Europe reforms its fisheries," *Nature*, vol. 498, pp. 17–18, June 2013.

51. D. P. Tittensor, M. Walpole, S. Hill, D. Boyce, G. L. Britten, N. Burgess, S. H. M. Butchart, and E. Reagan, "A mid-term analysis of progress towards international biodiversity targets," *Science - Under Review*, 2014.

52. M. Scheffer, S. Carpenter, J. A. Foley, C. Folke, and B. Walker, "Catastrophic shifts in ecosystems.," *Nature*, vol. 413, pp. 591–6, Oct. 2001.

53. K. a. Vert-pre, R. O. Amoroso, O. P. Jensen, and R. Hilborn, "Reply to Szuwalski: Policies robust to uncertainty in causes of productivity changes are needed," *Proceedings of the National Academy of Sciences*, vol. 110, pp. E1437–E1437, Mar. 2013.

54. G. L. Britten, M. Dowd, and B. Worm, "Environmental change drives declining recruitment capacity in global fish stocks," *Nature - Under Review*, 2014.

55. T. J. Quinn and R. B. Deriso, *Quantitative Fish Dynamics*. New York, NY: Oxford University Press, 1999.

56. E. K. Pikitch, C. Santora, E. A. Babcock, A. Bakun, R. Bonfil, D. O. Conover, P. Dayton, P. Doukakis, D. Fluharty, B. Heneman, E. D. Houde, and J. Link, "Ecosystem-based fishery management," *Science*, vol. 305, no. July, pp. 346–347, 2004.

57. P. Taylor, R. C. Francis, M. A. Hixon, M. E. Clarke, S. A. Murawski, S. Ralston, and M. Elizabeth, "Ten Commandments for Ecosystem-Based Fisheries Scientists," *Fisheries*, vol. 32, no. 5, pp. 37–41, 2011.

58. C. J. Walters and R. Hilborn, "Adaptive control of fishing systems," *Journal of the Fisheries Research Board of Canada*, vol. 33, pp. 145–159, 1976.

59. R. Mohn, "Personal communication," 2014.

60. W. Fennel, "Towards bridging biogeochemical and fish-production models," *Journal of Marine Systems*, vol. 71, pp. 171–194, May 2008.

61. M. J. Fogarty, "The art of ecosystem-based fishery management," *Canadian Journal of Fisheries and Aquatic Sciences*, vol. 490, no. November 2013, pp. 479–490, 2014.

62. B. DeYoung, M. Heath, F. Werner, F. Chai, B. Megrey, and P. Monfray, "Challenges of modeling ocean basin ecosystems.," *Science*, vol. 304, pp. 1463–6, July 2004.

63. J. P. Mattern, K. Fennel, and M. Dowd, "Estimating time-dependent parameters for a biological ocean model using an emulator approach," *Journal of Marine Systems*, vol. 96-97, pp. 32–47, Aug. 2012.

64. M. Dowd, "A sequential Monte Carlo approach for marine ecological prediction," *Environmetrics*, vol. 17, pp. 435–455, Aug. 2006.

65. J. Parslow, N. Cressie, E. P. Campbell, E. Jones, and L. Murray, "Bayesian learning and predictability in a stochastic nonlinear dynamical model.," *Ecological applications*, vol. 23, pp. 679–98, June 2013.

66. J. P. Mattern, K. Fennel, and M. Dowd, "Periodic time-dependent parameters improve forecasting abilities of biological ocean models," *Geophysical Research Letters*, vol. Accepted, pp. 1–5, 2014.

67. M. Travers, Y. Shin, S. Jennings, E. Machu, J. A. Huggett, J. G. Field, and P. M. Cury, "Two-way coupling versus one-way forcing of plankton and fish models to predict ecosystem changes in the Benguela," *Ecological Modelling*, vol. 220, pp. 3089–3099, Nov. 2009.

68. T. Lumley, "rmeta: Meta-Analysis. R Package version 2.16," 2012.